NASA TECHNICAL TRANSLATION NASA TT F-15,706

EXPERIMENTAL INVESTIGATION OF THE FLOW FIELD OF A HOT TURBULENT JET WITH LATERAL FLOW

PART II

L. Harms

Translation of "Experimentelle Untersuchungen über das Strömungsfeld eines heissen, turbulenten Strahles bei Queranströmung", Teil II. Deutsche Forschungs - und Versuchsanstalt für Luft - und Raumfahrt E.V. ZNW, Goettingen, Germany, Report 1-B 157-73 A 21, 28 September 1973, 50 pp.

NATIONAL AERONAUTICS AND SPACE ADMINISTRATION
WASHINGTON, D. C. 20546 JUNE 1974

STANDARD TITLE PAGE

1. Report No.	2. Government Accession No.	3. Recipient's Catalog No.
NASA TT G-15,706		

4. Title and Subtitle	5. Report Date
EXPERIMENTAL INVESTIGATION OF THE FLOW FIELD OF A HOT TURBULENT JET WITH LATERAL FLOW PART II	June 1974
	6. Performing Organization Code
7. Author(s)	8. Performing Organization Report No.
L. Harms	10. Work Unit No.
9. Performing Organization Name and Address SCITRAN Box 5456 Santa Barbara, CA 93108	11. Contract or Grant No. NASw-2483
	13. Type of Report and Period Covered Translation
12. Sponsoring Agency Name and Address National Aeronautics and Space Administration Washington, D.C. 20546	14. Sponsoring Agency Code

15. Supplementary Notes Translation of "Experimentelle Untersuchungen über das Strömungsfeld eines heissen, turbulenten Strahles bei Queranströmung", Teil II, Deutsche Forschungs - und Versuchanstalt für Luft - und Raumfahrt E.V. ZNW, Goettingen, Germany, Report 1-B 157-73 A 21, 28 September 1973, 50 pp.

16. Abstract

The flow field of a hot round jet in a cross wind has been investigated in the three meter wind tunnel of the DFVLR-AVA using a nine hole probe. The investigations were designed to produce information on the mixing processes of the jet and the cross flow, including the influence of temperature. For this purpose we measured the flow and temperature field of a heated round turbulent nozzle jet over several cross sections, at distances up to 30 nozzle diameters.

17. Key Words (Selected by Author(s))	18. Distribution Statement
	Unclassified - Unlimited

19. Security Classif. (of this report)	20. Security Classif. (of this page)	21. No. of Pages	22. Price
Unclassified	Unclassified	45	

TABLE OF CONTENTS

NOTATION LIST

Geometric Variables

b	Plate width
l	Plate length
D	Nozzle exit diameter
F_V	Valve cross section
F_D	Nozzle exhaust cross section
X,Y,Z,x,y,z	Cartesian coordinates
ϑ	Inclination of the nozzle jet axis with respect to the channel axis ($\vartheta = 90°$ for perpendicular incident flow)

Flow variables

a	Speed of sound
g	Local total pressure
$\dot{m}$	Mass flux
p	Local static pressure
p_a	Pressure at the outer side of the probe
p_o	Pressure at the top side of the probe
p_s	Pressure at the shaft side of the probe
p_t	Ambiant pressure
p_u	Pressure along the underside of the probe
q	Local stagnation pressure
V	Contribution of local velocity
V_∞	Incident flow velocity
V_j	Jet velocity at nozzle exit
V_x,V_y,V_z	x-y-z-components of local velocity
α_w	Angle between local flow direction and horizontal channel central plane (downwind angle)

β_w	Angle between local flow direction and x-z plane (sidewind angle).
Re_D	Reynolds number $Re = V_\infty \cdot D/\nu$; ν = kinematic viscosity.
Ma_D	Mach number $Ma = V_j/a_j$

Other variables and abbreviations

t	Temperature in °Celsius
T	Absolute temperature
$\vartheta = T_j/T_\infty$	Temperature ratio of nozzle jet and surroundings
$\psi = V_j/V_\infty$	Ratio of velocities of nozzle jet and incident flow
$\phi = (\rho_j V_j^2)/(\rho_\infty V_\infty^2)$	Ratio of momentum fluxes of nozzle jet and incident flow (momentum ratio)
$\varphi = \alpha_w/\vartheta$	Ratio of local flow direction α_w and nozzle inclination angle ϑ
$\Delta p_\beta = p_a - p_s$	Pressure difference due to sidewind
$\Delta p_\alpha = p_o - p_u$	Pressure difference because of downwind

Subscripts

m	Uncorrected measured value
j	Value referred to jet at nozzle exit
x,y,z	Value in direction of coordinate axis x, y, z
∞	Undisturbed flow
M	Value at center of jet
H	Value at electrical heater
R	Value in front of nozzle exit point
1. 2. 3....	Measurement point subscript

EXPERIMENTAL INVESTIGATION OF THE FLOW FIELD OF A HOT TURBULENT JET WITH LATERAL FLOW*

PART II

L. Harms

/7**

1. INTRODUCTION

Mixing processes between two crossing flows are very fundamental in fluid mechanics. In most of these mixing processes we have the case in which both flows differ greatly as to velocity, direction, mass or temperature. A round jet in a transverse flow is a typical example of such a flow, which can be encountered in various areas of technology.

It is very important to have information on the behavior of engine jets [1] for the design of jet supported short takeoff and vertical takeoff aircraft. The emerging engine jets are deflected by the flight wind and are deformed, and in the vicinity of the jets there are large induced interference forces which act on the aircraft body [2]. These forces have a detrimental effect on the performance and stability of the aircraft, especially during the landing and takeoff phase.

---

* German Research and Test Facility for Aerodynamics and Space Flight. Central Division for Low Velocity Wind Tunnels. Braunschweig-Göttingen·Porz-Wahn. Contract: 157/110/3/01/02. Presented at Colloquium for DGLR Specialists Group "Rigid Wing Aircraft" on December 6, 1973 in Porz-Wahn. Institute Director - Professor H. Schlichting.

** Numbers in the margin indicate pagination of original foreign text.

Another example of mixing processes which occur with jets in oblique cross loads is the cooling problem of walls which are subjected to hot gas flows. For example, in engine construction, the walls are cooled by expelling cold air from cold walls [3]. Similar conditions are found in spacecraft under hypersonic flight conditions [4] where cooling agents are expelled through perforated walls into the wall boundary layer. Even though several jets are required for an effective cooling, it is necessary to clarify the basic flow processes using a single jet. The simulation of different temperatures of the nozzle jet and the transverse flow can be easily carried out by heating the nozzle jet in experiments. It can be assumed that the results on propagation processes of heated jets then can be transferred to cooling problems in the correct manner.

The knowledge of the variation and mixing of the jet in a cross flow is also known from problems encountered in environmental science [5]. Here we are interested in the propagation of smoke fumes from chimneys into the atmosphere and the mixing of warm cooling water flows in rivers [6].

Because of the importance of jet flows in cross winds for a large number of applications, a number of investigations have been carried out with unheated jets. The dissertation of Chang [7] for jets in a transverse flow includes some of the first theoretical work. The experimental results obtained in conjunction with the development of VTOL aircraft on the jet in a cross wind are summarized in [8]. /6

P. T. Wooler, G. H. Burghart and J. T. Gallagher [9] considered the interaction between the jet and the crosswind by means of the friction resistance of a cross wind and the mass suction of the jet when they developed a model for the flow of the jet in a cross wind. They had to use empirical models for the mass suction and the momentum from experiments by J. F. Keffer and W. D. Baines [10]

and by R. Jordinson [11]. In a paper by H. Schmitt [12], new approaches for mass suction are presented and the empirical constants include measurement results on the jet width and average jet velocity.

Not much information is available on the behavior of hot jets. The present investigation will clarify the influence of temperature or density on the flow field of a round jet in a cross flow. For this purpose, we investigated the jet propagation of a heated jet for various velocity and momentum ratios with cross flow at the three meter wind tunnel of the DFVLR-AVA Göttingen. The measurements discussed here were carried out between July 10 and July 30, 1973.

2. EXPERIMENTAL CONFIGURATION

A jet nozzle is installed in the test section of the three meter wind tunnel of the DFVLR-AVA Göttingen [13], which has the capability of expelling heated air. The channel cross section is three meters and makes it possible to investigate jet propagation for a nozzle diameter of 5 cm.

This means that for wind velocities up to $V_\infty = 50$ m/s it is / 9
possible to have Reynolds numbers of up to $Re = V_\infty D/\nu =$ $1.7 \cdot 10^5$ referred to the nozzle diameter of $D = 5$ cm. The jet nozzle is installed at a distance of two meters from the wind tunnel nozzle on the sting balance carrier. Figure 1a shows a photograph of the test configuration. In the program we can see the electrical heater through which the air is directed to the jet nozzle. In the measurement series presented here, we installed a plane screening plate 0.75 m wide and 1.1 m deep at the nozzle exit point, so as to provide for a parallel flow in the vicinity of the nozzle (Figure 1b). In front of the capture funnel of the wind tunnel we have the probe displacement device with the nine hole

probe. The schematic experimental configuration including the measurement collection unit is shown in Figure 2. The expelled air is supplied by a screw compressor installation of the DFVLR-AVA [14] at a pressure of p_t = 2.8 bar. This pressure is maintained constant through a pressure regulation valve. The compressed air reaches the speed of sound at the narrowest point of the dosing valve. By adjusting the central body of the dosing valve it is possible to regulate the expelled amount. After this the air runs through an electrical heater. The air can be heated up to a temperature of t_H = 400° C. The control of the heating power is done by means of a 400 kW Leonard unit which is remotely controlled from the measurement cabin.

The flow field was measured using a nine-hole probe (Figure 3). This probe measured the total pressure g, the flow angle α_w, the sidewind angle β_w and the static pressure p. The pressure difference $\Delta p_\alpha = p_o - p_u$ is proportional to the inclination angle α_w. The sidewind angle β_w is found from the pressure difference $\Delta p_\beta = p_a - p_s$ between two pressure taps opposing each other and the measured stagnation pressure $q_m = g_m - p_m$ using a calibration curve [15]. The local stagnation pressure q and the static pressure are determined for oblique wind conditions using calibration curves [15]. Pressures measured by the nine hole probe are converted to electrical voltages using differential pressure measurement cells with a measurement range of 0.5 bar and 0.1 bar, respectively (Figure 4). The output voltages of these pressure measurement cells are amplified and are averaged in integrating digital volt meters over two seconds. The deviation of the inclination angle-pressure difference $\Delta p_\alpha = p_o - p_u$ from the value zero is used to control the stepping motor of the inclination angle displacement unit of the probe displacement unit, so that the probe automatically turns into the wind. /10

A thermoelement is installed in the probe and its output voltage is amplified just like that of the pressure measurement cells and this is displayed in a digital volt meter. The measured values of pressure and temperatures are recorded on an eight-channel tape. The test installation with data collection unit is shown in Figure 2.

3. EXECUTION AND EVALUATION OF RESULTS

In the present part of the investigation we adjusted an exhaust velocity of the unheated nozzle jet of V_j = 180 m/sec while maintaining the amount of expelled air constant. By controlling the wind tunnel velocity, we adjusted jet velocity to incident flow velocity ratios of up to $\varphi = V_j/V_\infty = 11.3$, corresponding to momentum ratios of $\Phi = (\rho_j V_j^2)/(\rho_\infty V_\infty^2) = 64$. The experiments with the heated jet were only carried out after adjusting a constant temperature t_H = 350° C in the heater and the temperature of t_R = 300° C in the expulsion nozzle. The available compressor installation can also be used to investigate the critical (Ma_D = 1) and over-critical (Ma_D > 1) nozzle jets by increasing the compressor pressure.

The measurement of the flow field is carried out in sections perpendicular to the channel axis for various displacements x/D from the center of the jet nozzle. Depending on the displacement, a range of up to 1 m^2 was measured with distances between measurement points of between 50 and 100 mm.

The measurements are evaluated using a FORTRAN computer program for the electronic computer installation IBM 360/65. /11

The computer program determines the resulting local velocity V (Figure 5), its components V_x, V_y, V_z in the three coordinate directions x, y and z and the flow angles α_w and β_w from the

measured data. The local jet temperature is normalized using the wind tunnel jet temperature and is printed out. The results are given in lists and on punched cards.

Special plotting programs were written for the CALCOMP plotter in order to present the results in various methods of representation. /12

4. RESULTS

4.1. Flow observation

The flow photographs (Figure 6) show the round nozzle jet in a cross wind for a Reynolds number of the nozzle flow of $Re_D = \frac{V_j \cdot D}{\nu} = 15 \cdot 10^5$. This Reynolds number is high above the critical Reynolds number $Re_D = 2300$, below which we do not have any turbulent nozzle flow, and produces a jet expansion shortly after leaving the nozzle exit point. Even for a small cross velocity there is intensive mixing in the vicinity of the jet nozzle as well as a strong deformation of the jet. The potential core of the jet is destroyed already after a few nozzle diameters, and we can no longer speak of a connected jet cross section.

During the subsequent measurement of the flow field, it is necessary to know that there are approximately periodic fluctuations [16] in the turbulent mixing region which must be investigated and require special care when being measured.

4.2. Velocity distribution in the jet without a crosswind

Velocity distribution at the exit cross section of the conical nozzle used is shown in Figure 7. The velocities V in the jet refer to the jet axis velocity V_M and we have plotted the dimension-

less values V/V_M as a function of the distance to the axis y/D. At a distance of 0.1 nozzle diameters, the nozzle has a rectangular velocity profile, which varies hardly at all from the distribution for a corrected nozzle [15]. As the distance z/D from the nozzle mouth is increased, the profiles become flatter. After a distance of six nozzle diameters, they have a similar distribution according to the shape of the Gaussian normal distribution. After this distance we can speak of a completely developed free jet. The heating of the jet to a temperature of t_j = 300° C corresponding to a temperature ratio of $\Theta = T_j/T_\infty = 2$, brings about a stronger sideways propagation of the hot jet, i.e., a somewhat greater half value radius $R_{0.5}$. The velocity distribution V/V_j along the jet axis is shown in Figure 8 and indicates the beginning of a completely developed free jet at a distance of 6 nozzle diameters. Here again for the conical nozzle unit we find no noticeable differences in the velocity decrease along the jet axis z/D as compared with the measurements with corrective nozzles [15]. The heating of the jet therefore seems to cause a stronger jet mixing with the surroundings so that here the decrease in the axial velocity v_M is somewhat faster than for the cold jet. Compared with the results of S. Corrsin [17], we measured somewhat larger velocities.

4.3. Velocity distribution in the jet with a crosswind

Using a a plotting program we plotted the velocities V divided by the incident velocity V_∞ and show the lines of equal velocity V/V_∞ = const (isotachs), (Figures 9 to 12). In order to show the distance between the jet field and the nozzle exit point, we also show the nozzle to scale in these diagrams.

Already after a short distance of 4 nozzle diameters, we can see the deformation of the jet cross section (Figure 9) with the isotachs for a momentum ratio of $\phi = 64$. We already see a clear horseshoe shape of the jet cross section.

As the distance x/D from the nozzle increases, two velocity maxima are formed depending on the magnitude of the momentum ratio ϕ. As we will later on show, this coincides with the position of two vortex centers (Figures 10 to 12).

4.4. Temperature distribution in the jet with a crosswind /14

Local temperatures T are made nondimensional using the maximum temperatures T_{max} which occur in the cross section. The curves of equal temperature T/T_{max} = const (isotherms) are shown to scale in addition to the nozzle exit point in the subsequent diagrams (Figures 13 to 16).

For the momentum ratio $\phi = 64$ investigated, the vortex development in the jet in a crosswind is so well developed that the temperature distribution takes on a form similar to the velocity distribution. The temperature maxima occur at the vortex centers. At the jet center line, which is often assumed to be the line of maximum jet velocity, we measured substantially lower temperatures.

4.5. Velocity vectors in the normal plane

The projection of the velocity vectors $\underline{v}/V_\infty$ on the y-z plane is shown in Figures 17 to 20 and gives a better idea of the flow processes which occur with a jet in a crosswind. For orientation, the figures also contain the nozzle exit point and a comparison vector having the magnitude $V_z/V_\infty = 0.1$ and these are drawn

to scale. All of the plots were made for the momentum ratio $\phi = 64$.

Already after a short distance of 4 nozzle diameters (Figure 17) the nozzle jet is deformed into a horseshoe shape cross section, and there is a vortex-like secondary flow at its extremities. As the distance increases x/D=7 (Figure 18a), these vortices develop even more. The centers of these vortex pairs which rotate in opposite directions move farther away from the nozzle exit point in the direction of the z axis as the distance is increased.

A comparison of the vector diagrams of the hot ($\theta = 2$) and the / 15
cold nozzle jet for the same momentum ratio $\phi = 64$ and for the distances x/D = 7 (Figure 18a and 18b) and x/D = 15 (Figures 19a and 19b) shows that the structure of the jet cross section is maintained in the form of two opposing vortex pairs. Also the distance z of the vortex centers from the nozzle mouth is not influenced by the temperature. The differences between the flow fields of cold and hot jets with the same momentum ratio ϕ seems only to be expressed by a greater propagation of the vortex field of the hot jet. In the far field of the jet, after 30 nozzle diameters (Figure 20), a vortex pair can still be found even for the hot jet. This vortex pair is only consumed due to the action of friction of a greater distance.

4.6. Three-dimensional representation of the flow field

In order to give a clear representation of the flow field of a round jet in a crosswind, we present an isometric picture in three dimensions in the following diagrams (Figures 21-24). The y-z plane is represented by the coordinate axes y/D and z/D, and we have plotted the dimensionless velocity field $(V_x - V_\infty)/V_\infty$.

At small distances from the jet axis (Figure 21) we have a region of high over velocity $(V_x - V_\infty)/V_\infty > 1$ over the jet center line, which can be called the jet core. To the side of this core we have over velocities $V_x > V_\infty$ at the centers of the vortices. These over velocities, whose maxima coincide with the centers of the opposing vortex pair, surround a wake region in the symmetry plane (y/D=0) according to Figures 22a and 22b. The jet core can only be distinguished because of a small over velocity. The velocity fields of the hot and cold jet are very similar, if the same momentum ratio ϕ occurs. Even after a large distance /16 x/D=15 the similarity of the flow field of hot and cold jets in a crosswind remains (Figure 23a and 23b). In the far field (Figure 24) the velocities $(V_x - V_\infty)/V_\infty$ are greatly reduced but the vortex centers which are the region of maximum velocity, are maintained. These absorb the axial momentum of the jet and flow away in the direction of the jet axis.

4.7. Comparison with theoretical and experimental results of other authors

The variation of the found jet in the crosswind is often expressed by the variation of the jet axis, i.e., of the line of maximum velocity along the symmetry plane of the flow field. Figure 25 shows such a theoretical variation according to H. Schmitt [12] for cold jets for momentum ratio of $\phi = 64$. Experimental results of Keffer and Baines [10] and of Thompson [18] are also shown in this figure for cold jets for comparable momentum ratios of $\phi = 64$ and $\phi = 65.5$, respectively. In addition we also show the present results for hot and cold jets for the momentum ratio $\phi = 64$. The jet axis is characterized by the maximum in the V_x velocity. It can be seen that for smaller distances x/D from the nozzle, the theory and experiments of Keffer and Baines and of Thompson agree very well. For greater

distances, the experiments of Thompson result in a somewhat reduced reflection of the jet compared with the theory, which can only be partially explained by the somewhat greater momentum ratios which were used in the measurements of Thompson. The measurement point for cold jets which is a result of the present investigation, is very close to the measurement curve of Thompson. On the other hand, according to the present investigation, the measured values for a warm jet are closer to the theoretical curve./17

The coordinates x/D and z/D of the vortex centers of the opposing vortex pairs were determined in our investigation. These values are shown in the diagram for hot and cold jets for the momentum ratio $\phi = 64$. A curve was drawn through the values corresponding to hot jets. In addition, we also show the measured values of Thompson for the cold jet, but for a somewhat greater momentum ratio $\phi = 65.5$. With a somewhat greater momentum ratio, it is possible to partially explain the differences in the position of the measurement points of Thompson and our measurements. Compared with the variation of the jet axis, the vortex axis has a somewhat greater deflection due to the crosswind. The experimental results [15] show that the position of the vortex axis is unchanged for hot and cold jets with the same momentum ratio ϕ.

5. SUMMARY

The experimental investigations for cold (θ=1) and hot nozzle jets (θ = 2) in a crosswind have shown that the initial horseshoe deformation of the jet cross section of a round jet in a crosswind leads relatively soon to a formation of a vortex pair rotating in opposite directions. This vortex pair limits the deflected jet on both sides and absorbs the momentum of the jet.

For the same velocity ratio ν, the position of the vortex pairs is displaced according to the temperature ratio θ of the jet flow and the cross flow, towards smaller nozzle distances z/D. On the other hand, if the same momentum ratio ϕ is maintained for cold and hot jets, then the position of the vortex pair is essentially conserved. For the hot jet we find a greater expansion of the flow field, however.

Comparisons of the position of the vortex pairs with the corresponding investigations of other authors on the position of the maximum velocity along the symmetry line shows that there is a greater deflection of the opposing vortex pair.

6. REFERENCES

1. Williams, J. and Mairice N. Wood. Aerodynamic Interference Effects with Jet-Lift V/STOL Aircraft under Static and Forward Speed Conditions. RAE Technical Report No. 66403 1966.

2. Fütterer, H. and L. Harms. Jet Interference Measurements on a VTOL Model with Jet Simulation by Fans. AGARD Conference Proceedings No. 22, 1967, pp. 17/1-26.

3. Schetz, J. A. and F. S. Billig. Penetration of Gaseous Jets Injected into a Supersonic Stream. Journal of Spacecraft and Rockets. Vol. 3, No. 11, November, 1966, pp. 1658-1665.

4. Kush, E. A. and J. A. Schetz. Liquid Injection into a Supersonic Flow. AIAA/SAE 8th Joint Propulsion Specialist Conference AIAA Paper No. 72, 1972, p. 1180.

5. Parker, F. L. and P. A. Krenkel. Physical and Engineering Aspects of Thermal Pollution. CRC Critical Reviews in Environmental Control, Vol. 1, February, 1970, pp. 101-192.

6. Kennedy, V. S. and J. A. Mihursky. Bibliography of the Effects of Temperature in the Aquatic Environment. Submitted to Hearings on Thermal Pollution - 1968 before the Committee on Air and Water Pollution, U. S. Senate, February, 1968, Part I. pp. 471-568, GPO.

7. Chang, H. C. The Rolling Up of a Cylindrical Jet by a Crosswind. Dissertation, University Göttingen, 1942, pp. 1-52.

8. Margason, R. J. Jet-Wake Characteristics and Their Induced Aerodynamic Effects on V/STOL Aircraft in Transition Flight. NASA SP - 218, September, 1969 pp. 1-18.

9. Wooler, P. T., G. H. Burghart and J. T. Gallagher. Pressure Distribution on a Rectangular Wing with a Jet Exhausting Normally into an Airstream. J. Aircraft, Vol. 4, 1967, pp. 537-543.

10. Keffer, J. F. and W. D. Baines. The Round-Turbulent Jet in a Crosswind. Journal of Fluid Mechanics. Vol. 15, Part 4, 1963, pp. 481-496.

11. Jordinson, R. Flow in a Jet Directed Normal to the Wind. ARC, R + M, 3074, 1958.

12. Schmitt, H. Deflection of a Round Turbulent Free Jet in a Crosswind. DFVLR-AVA Report 061-72 A 24, 1972.

13. Fütterer, H., D. Mehmel and F. W. Riegels. Measurement Technology, Data Collection and Data Processing at the Large Wind Tunnels of the Aerodynamic Test Facility, Göttingen. Yearbook 1970 of DGLR, 1970, pp. 166-185.

14. Fütterer, H. and R. Wulf. Description of a Projected Compressor Installation for Producing Compressed Air for Expelled Air and Suction Tests in the Three-Meter AVA Wind Tunnel. AVA Report, 63 A 01, 1963.

15. Harms, L. Experimental Investigations of the Flow Field of a Hot, Turbulent Jet with Cross Flow. First Partial Report. DFVLR-AVA Report 157 73 A 18, 1973.

16. Laurence, J. Intensity, Scale and Spectra of Turbulence in Mixing Region of Free Subsonic Jet. NACA Report 1292, 1956.

17. Corrsin, S. Further Experiments on the Flow and Heat Transfer in a Heated Turbulent Jet. NACA Report 998, 1950.

18. Thompson, A. M. The Flow Induced by Jets Exhausting Normally from a Plane Wall into an Airstream. Ph.D. Thesis, University of London, September, 1971.

TABLE 1. MEASUREMENT PROGRAM

MR	φ	σ	x/D	ϵ	Photo No.
2010 - 2022	8	64	7	1	18b, 22b
2024 - 2041	8	64	15	1	19b, 23b
2079 - 2092	11,3	64	4	2	9, 13, 17, 21
2065 - 2078	11,3	64	7	2	10, 14, 18a, 22a
2048 - 2064	11,3	64	15	2	11, 15, 19a, 23a
2093 - 2104	11,3	64	30	2	12, 16, 20, 24

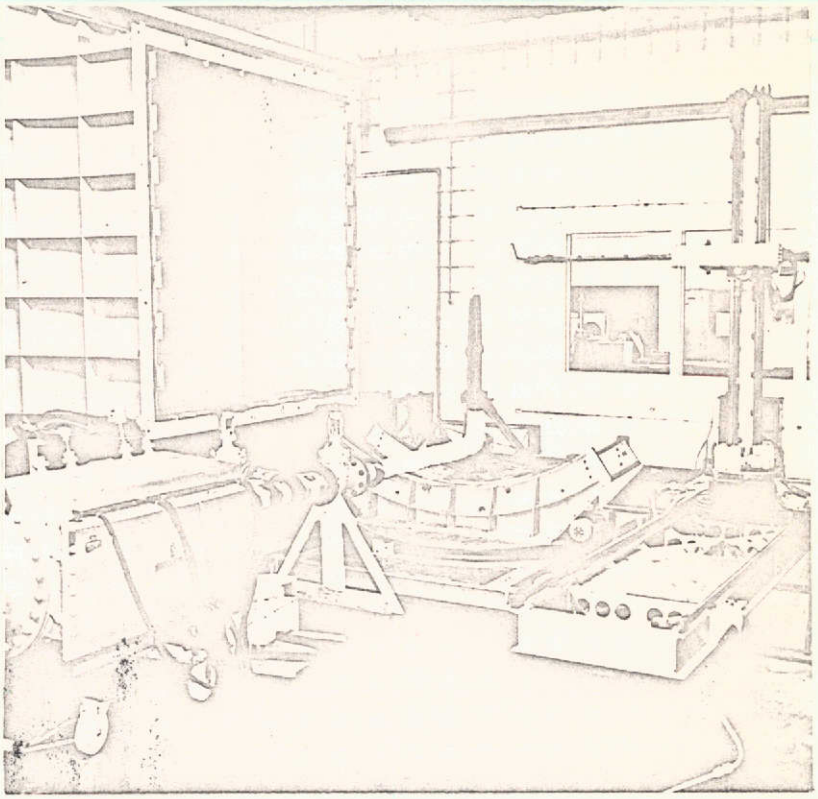

Figure 1a. Test installation without screening plate.

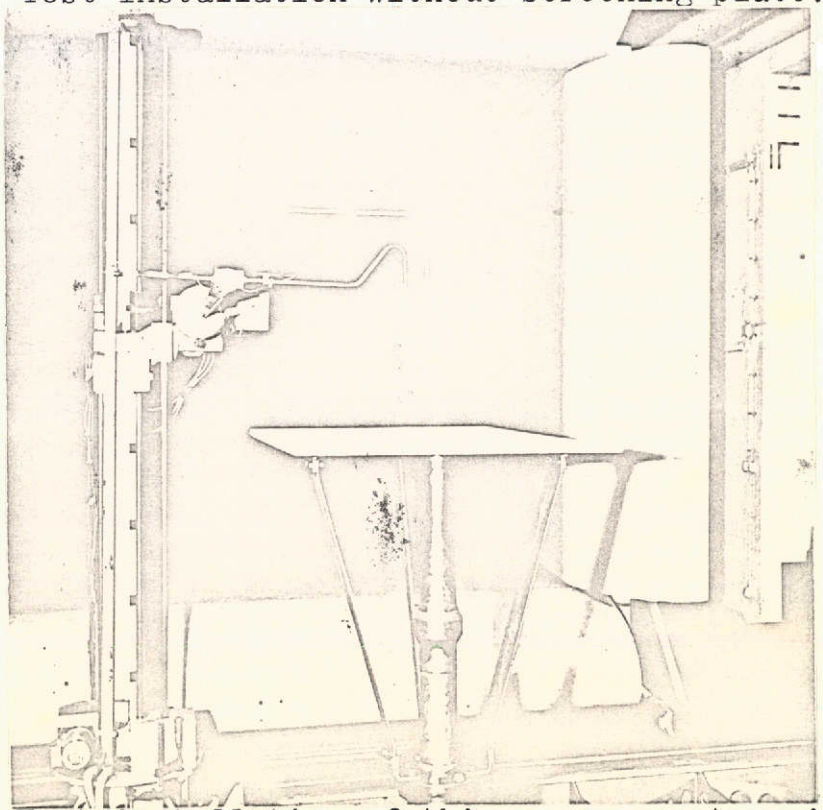

Figure 1b. Test installation of this measurement series with screening plate

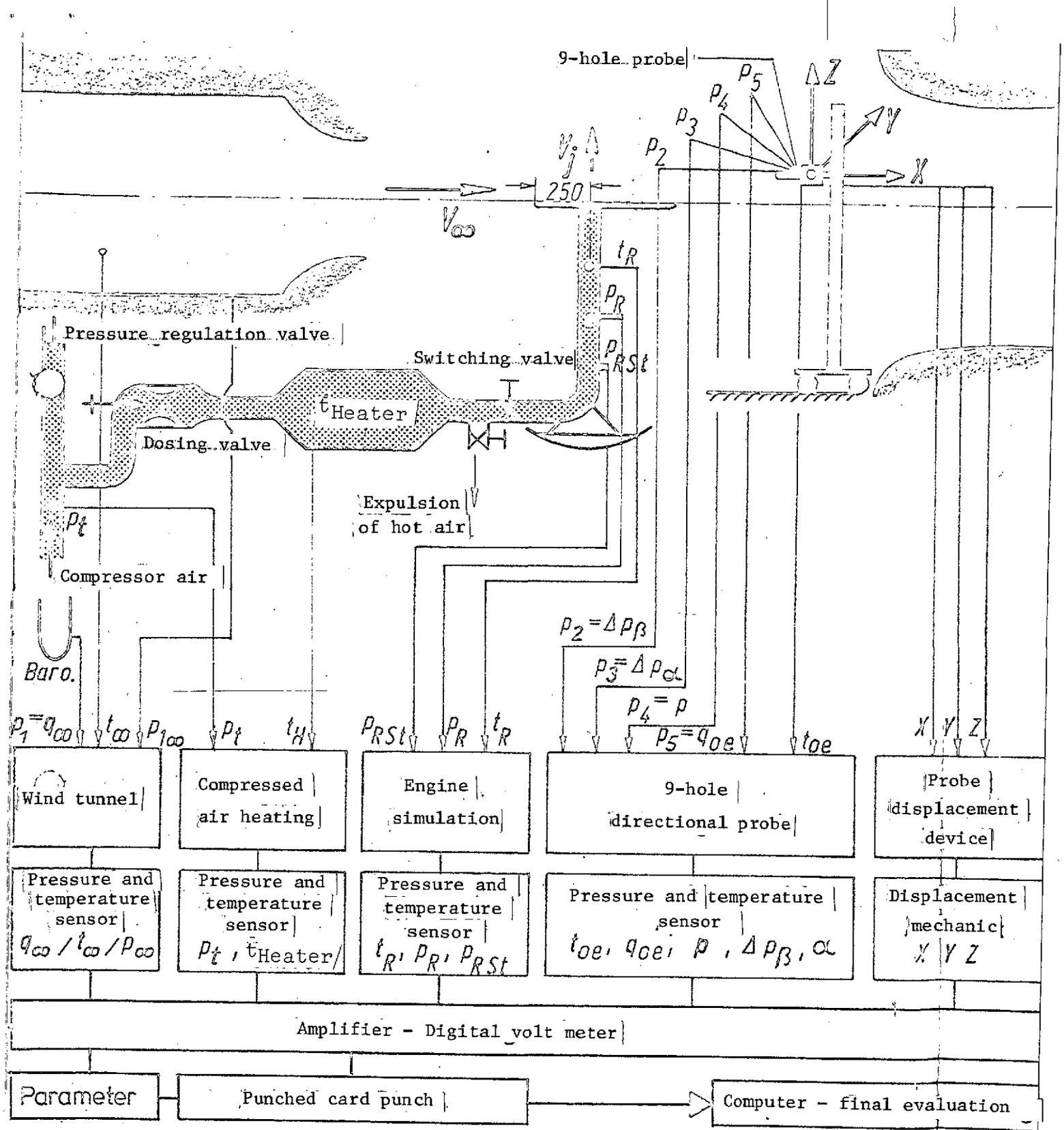

Figure 2. Test installation for jet simulation

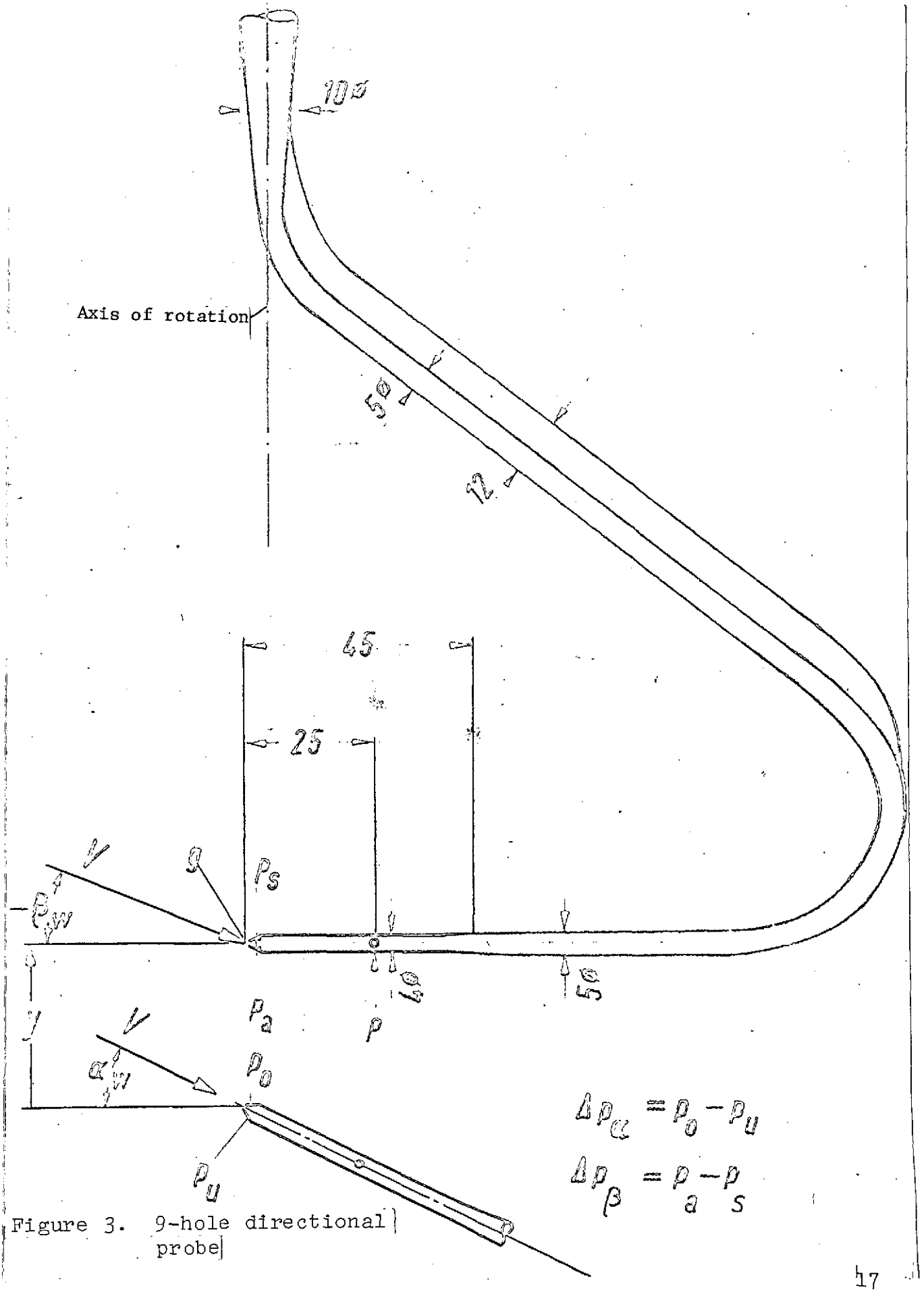

Figure 3. 9-hole directional probe

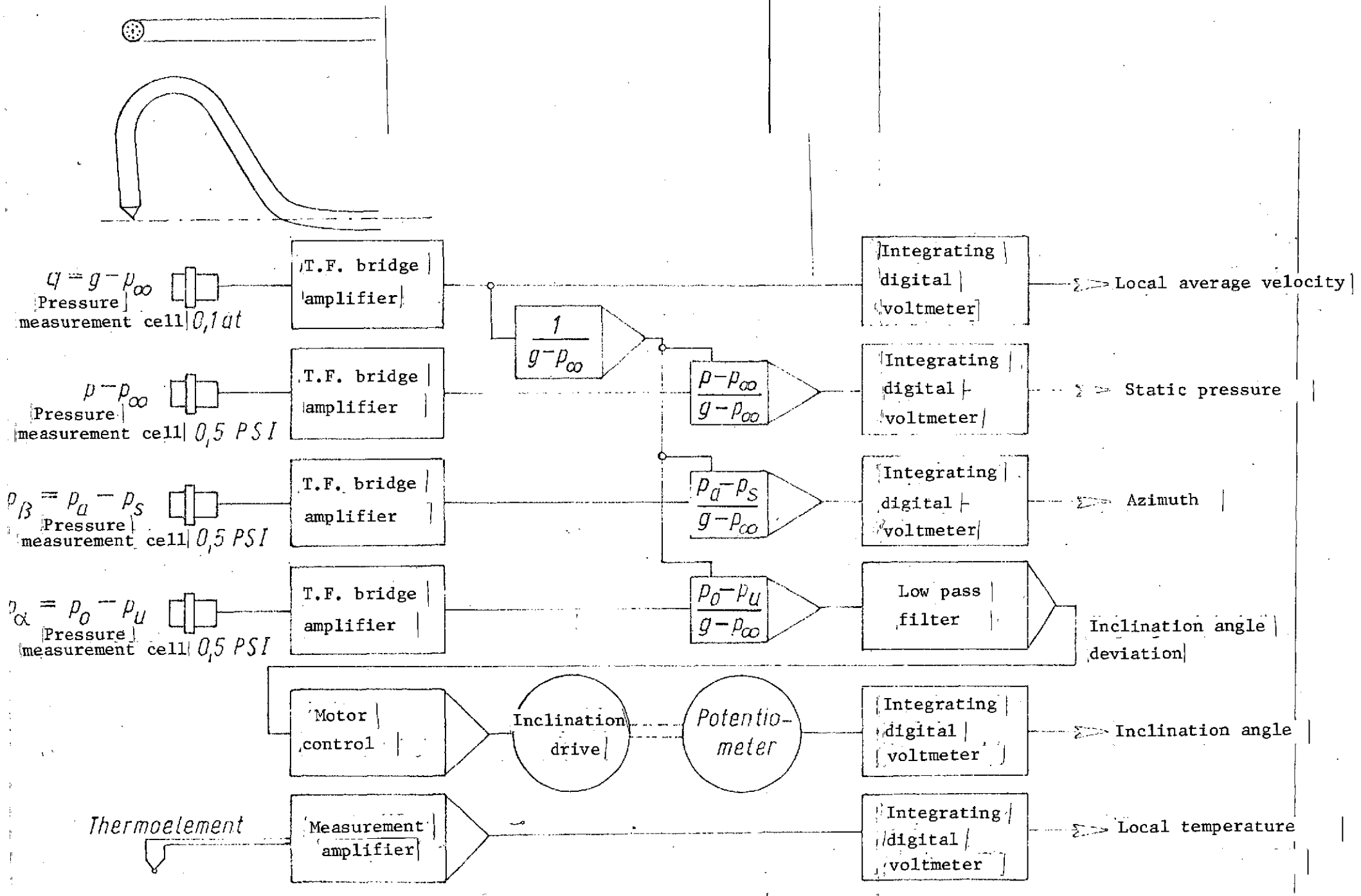

Figure 4. Flow field measurement in wind tunnel using 9-hole probe

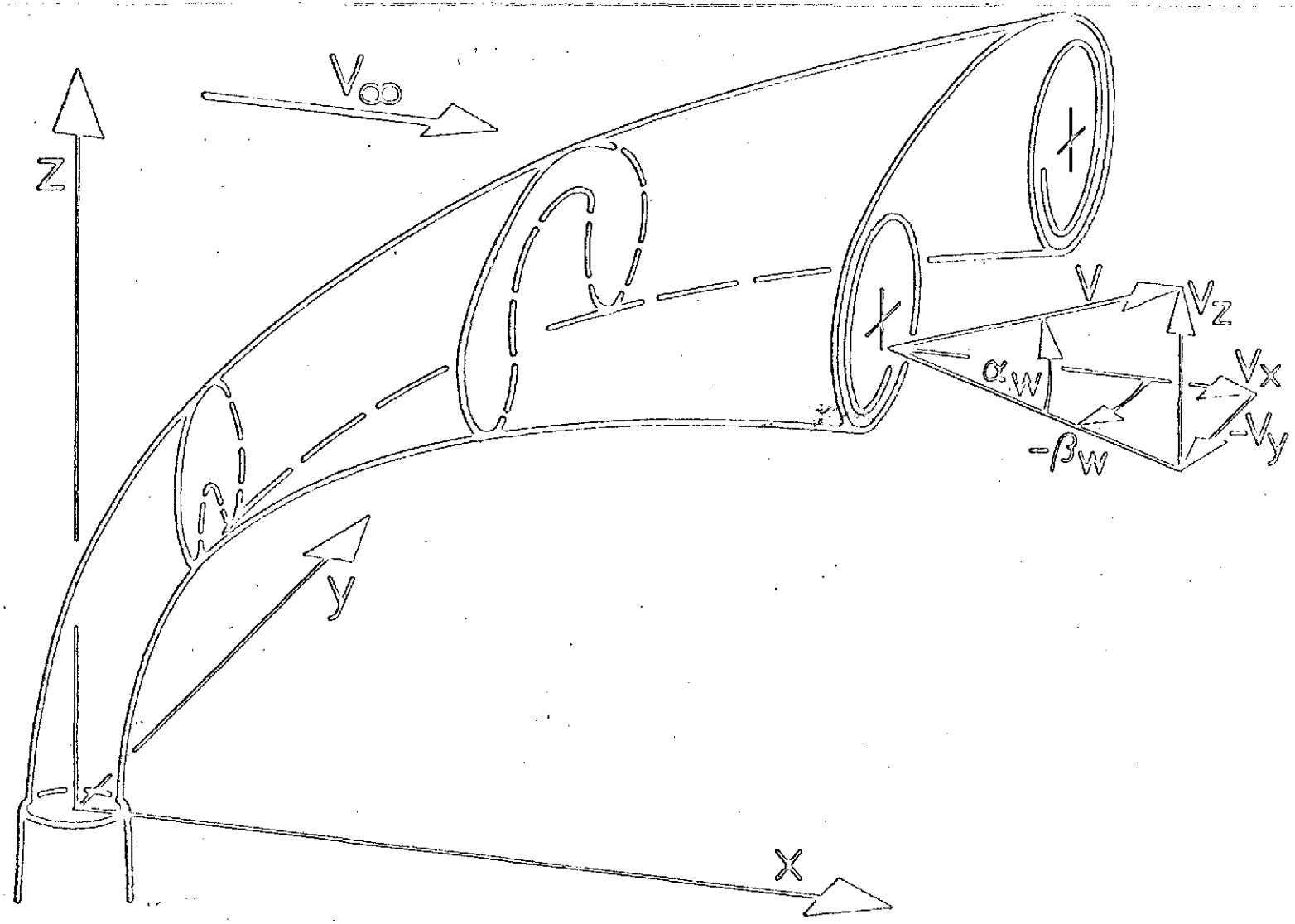

Figure 5. Coordinates and notation

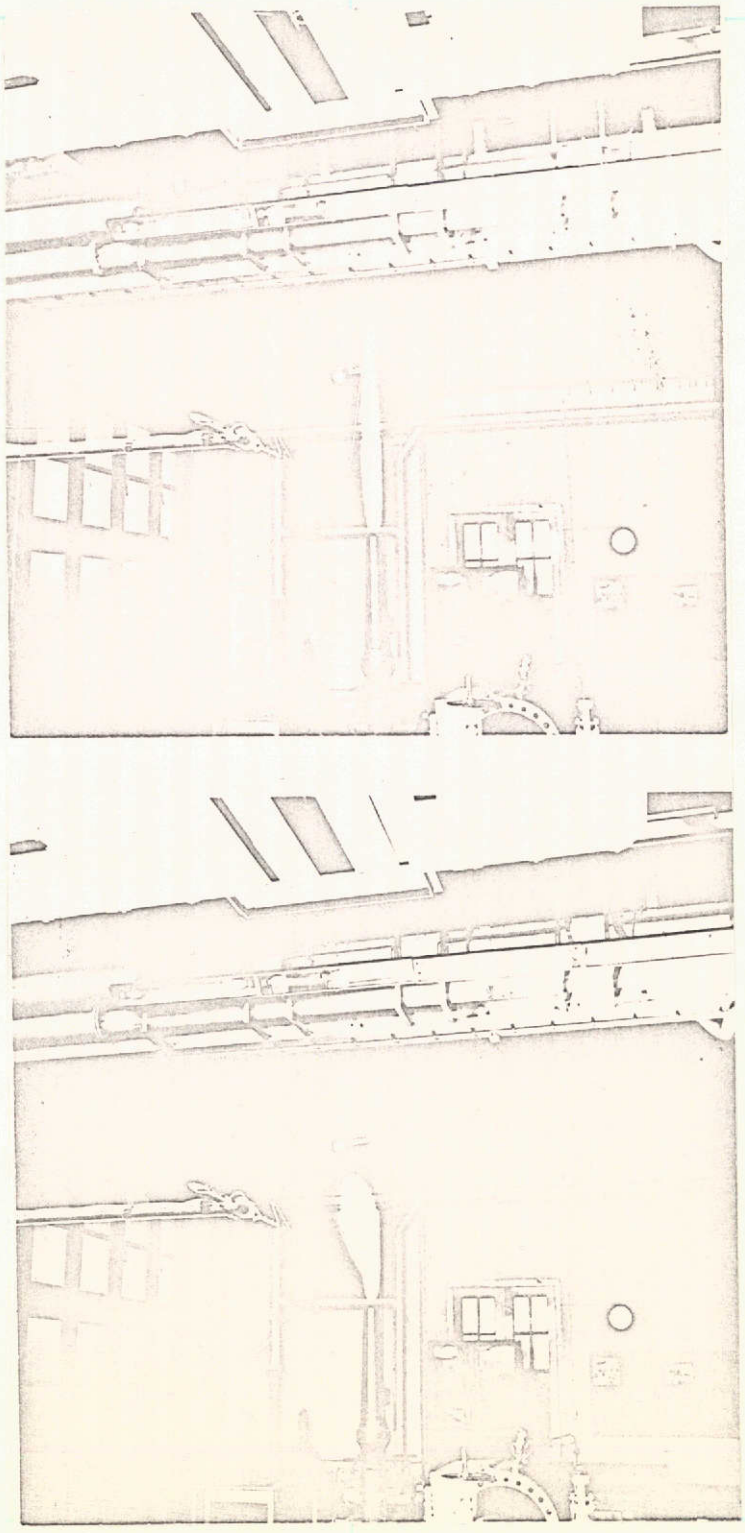

Figures 6a and 6b. Flow photographs of a jet with and without blowing

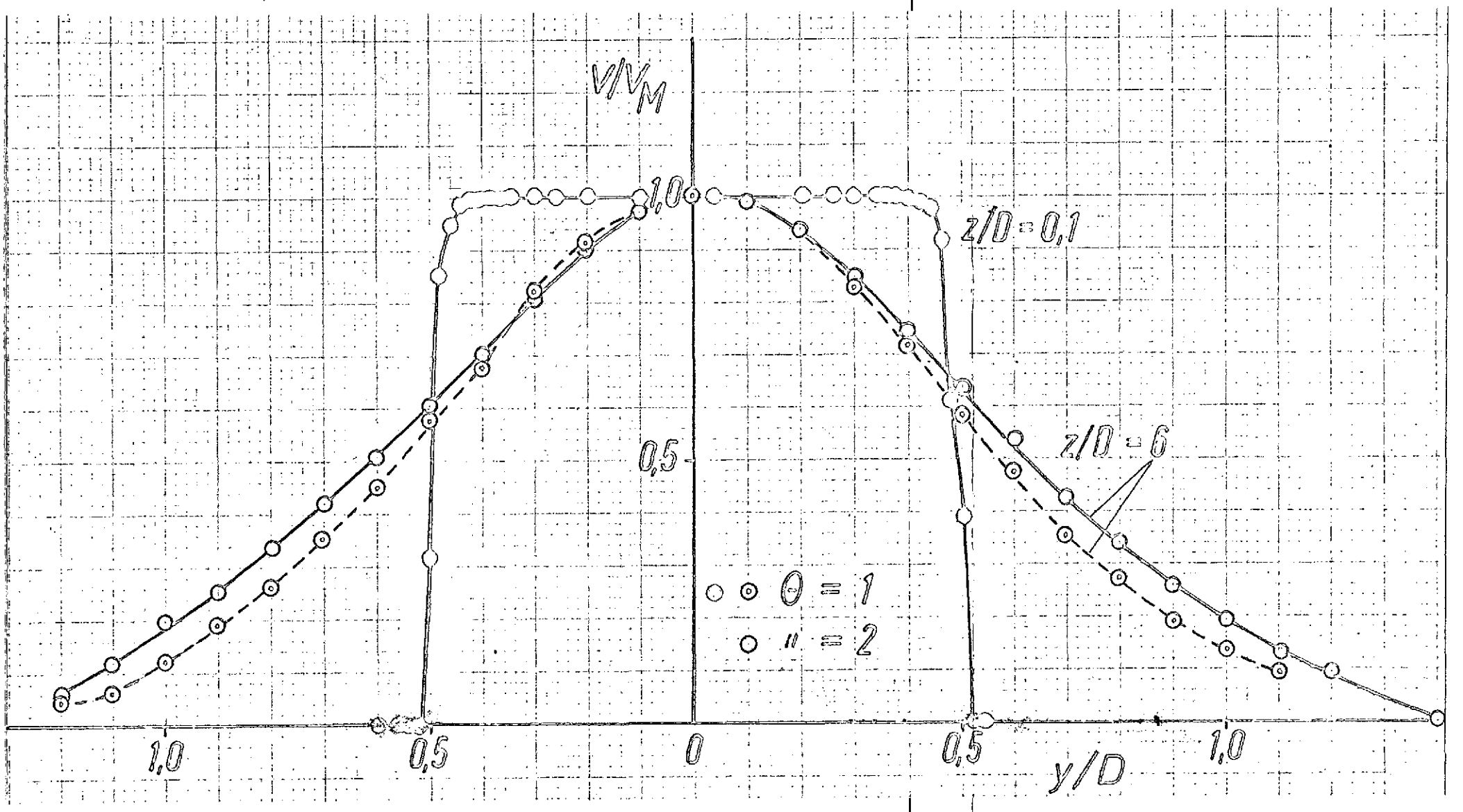

Figure 7. Velocity distribution perpendicular to jet axis

FOLDOUT FRAME
1

FOLDOUT FRAME
2

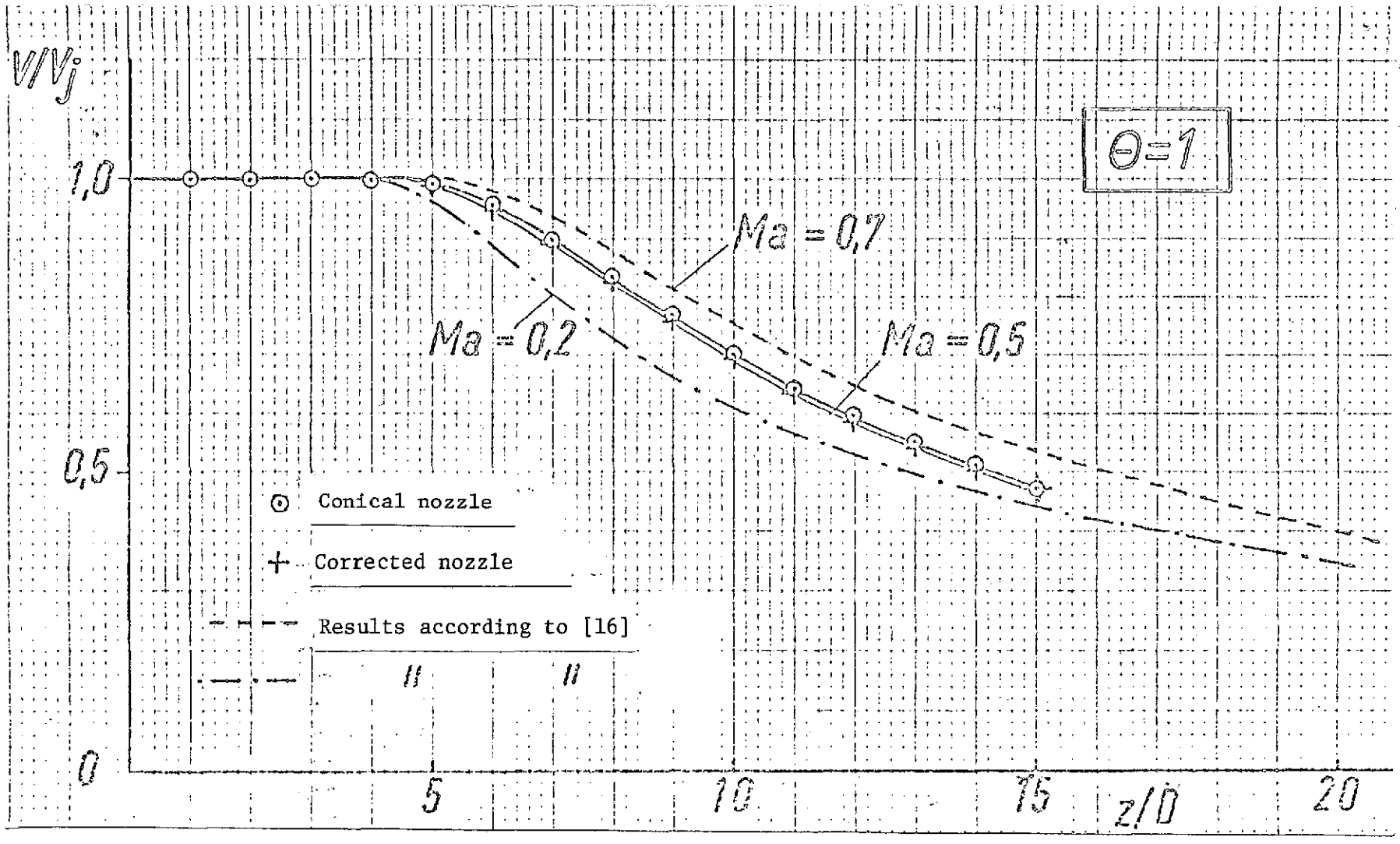

Figure 8. Velocity distribution along the jet axis for conical and corrected nozzle with the cold jet.

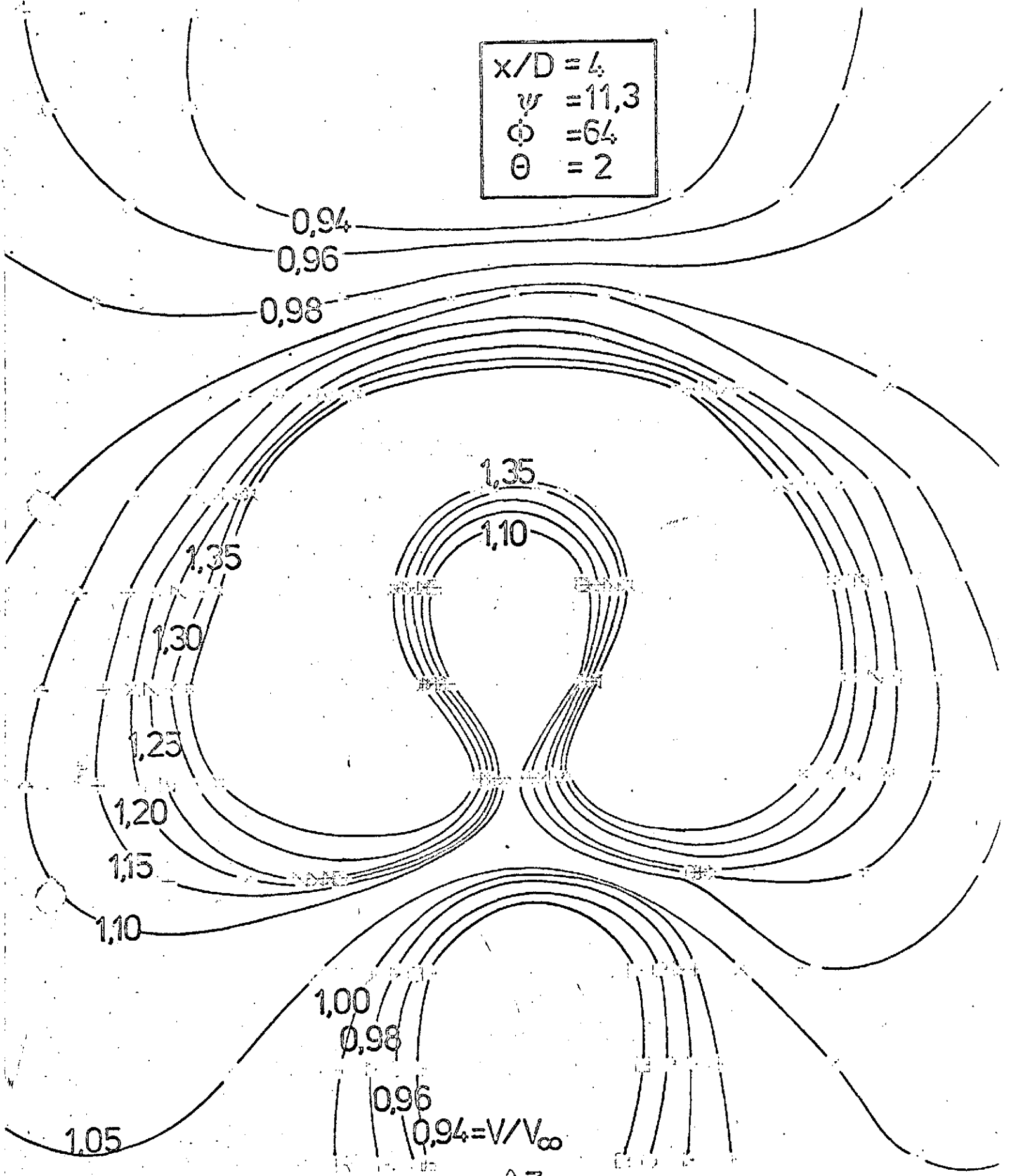

Figure 9. Velocity distribution in the transverse plane (y-z plane)
x/D = 4, ψ = 11,3; Φ = 64, Θ = 2

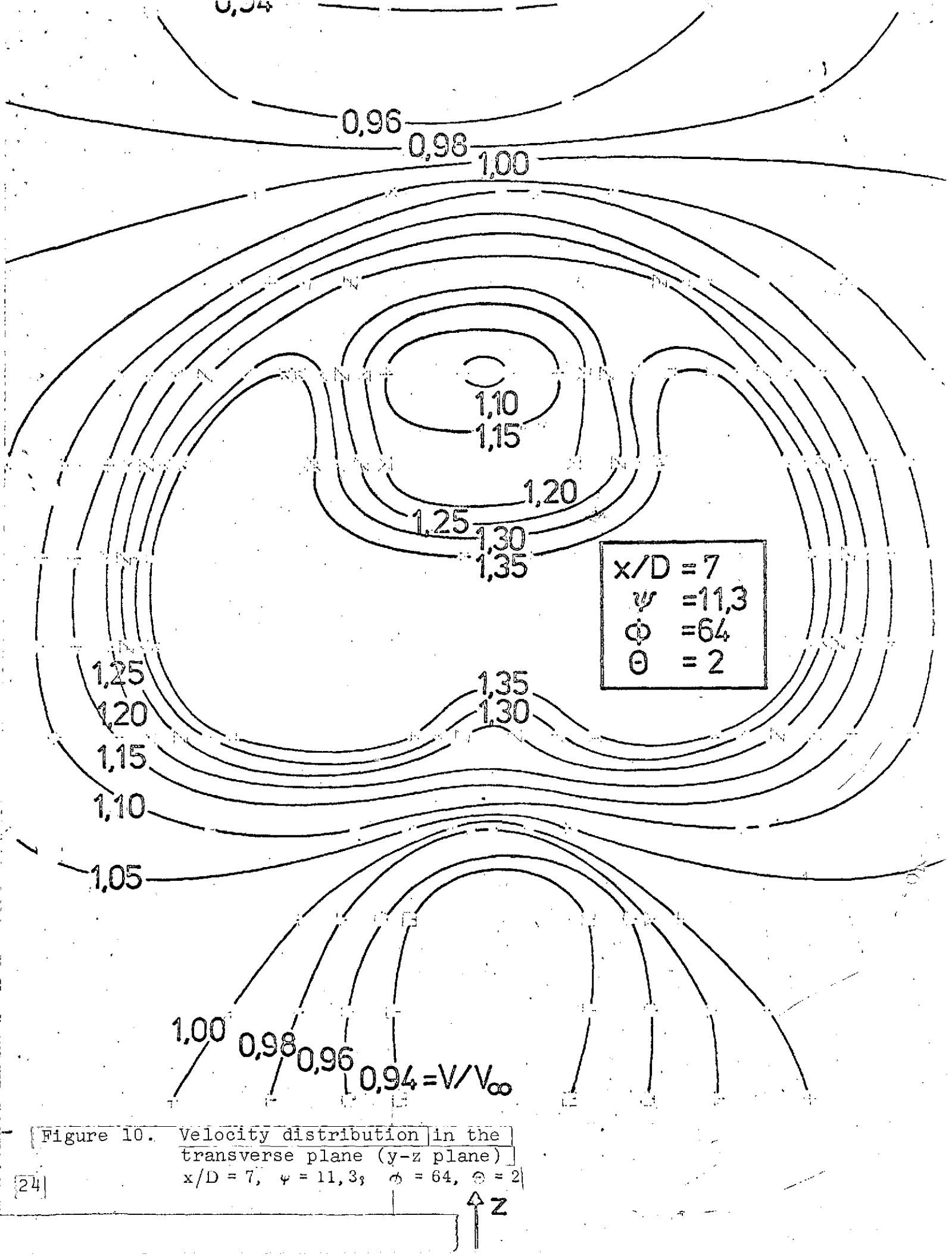

Figure 10. Velocity distribution in the transverse plane (y-z plane)
x/D = 7, ψ = 11,3; Φ = 64, Θ = 2

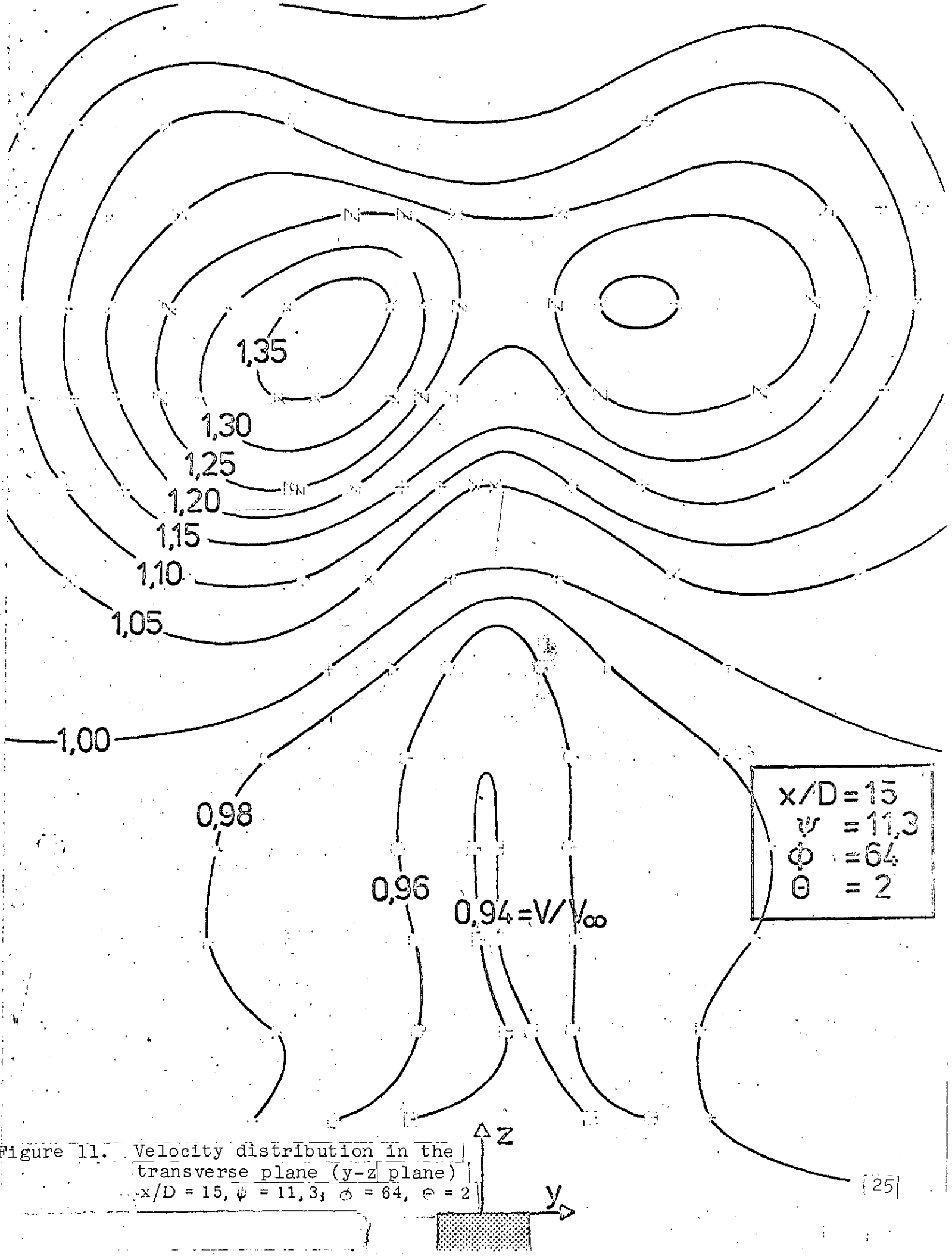

Figure 11. Velocity distribution in the transverse plane (y-z plane) x/D = 15, ψ = 11,3; ϕ = 64, Θ = 2

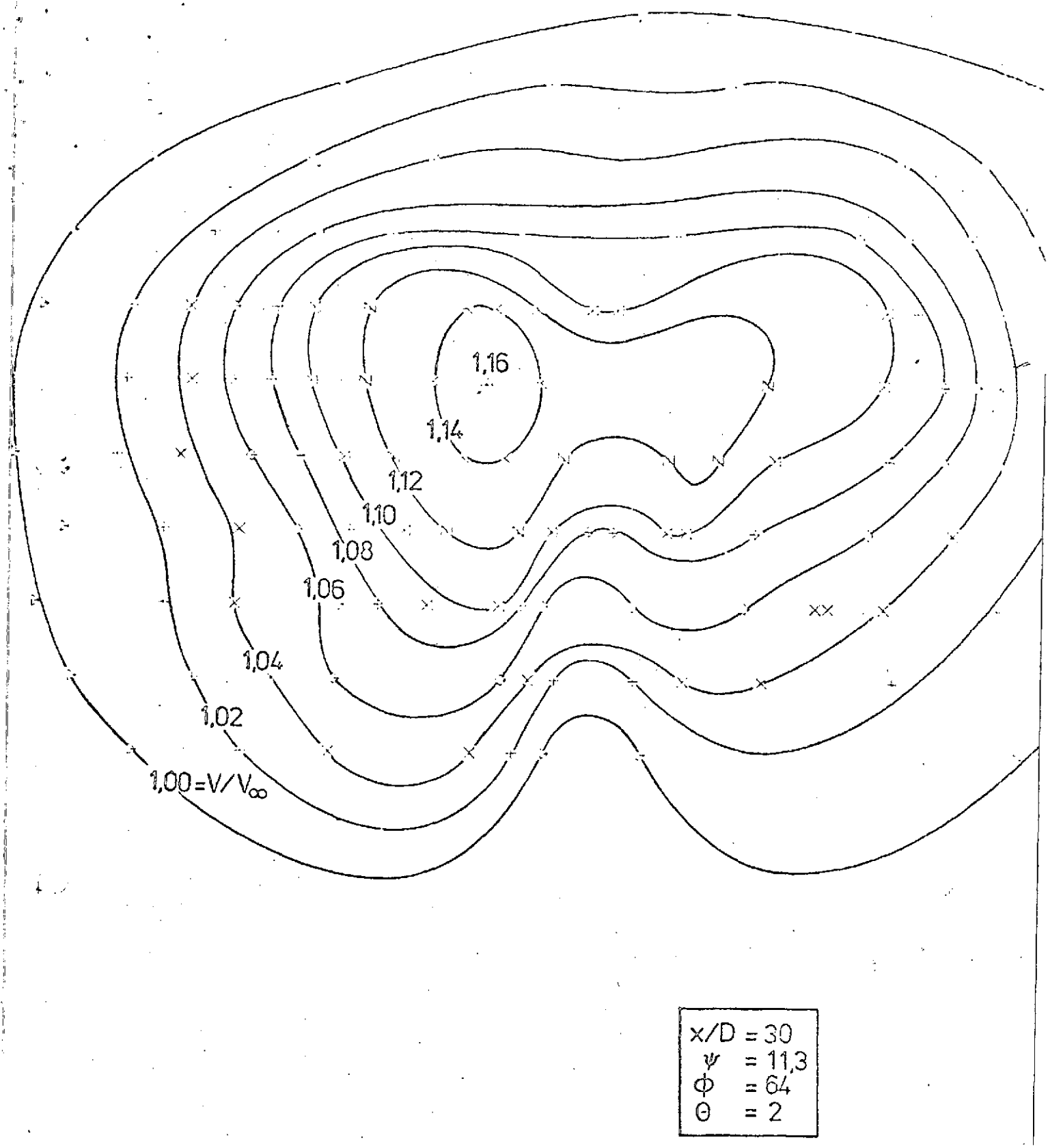

Figure 12. Velocity distribution in the transverse plane (y-z plane) $x/D = 30$, $\psi = 11,3$, $\phi = 64$, $\Theta = 2$

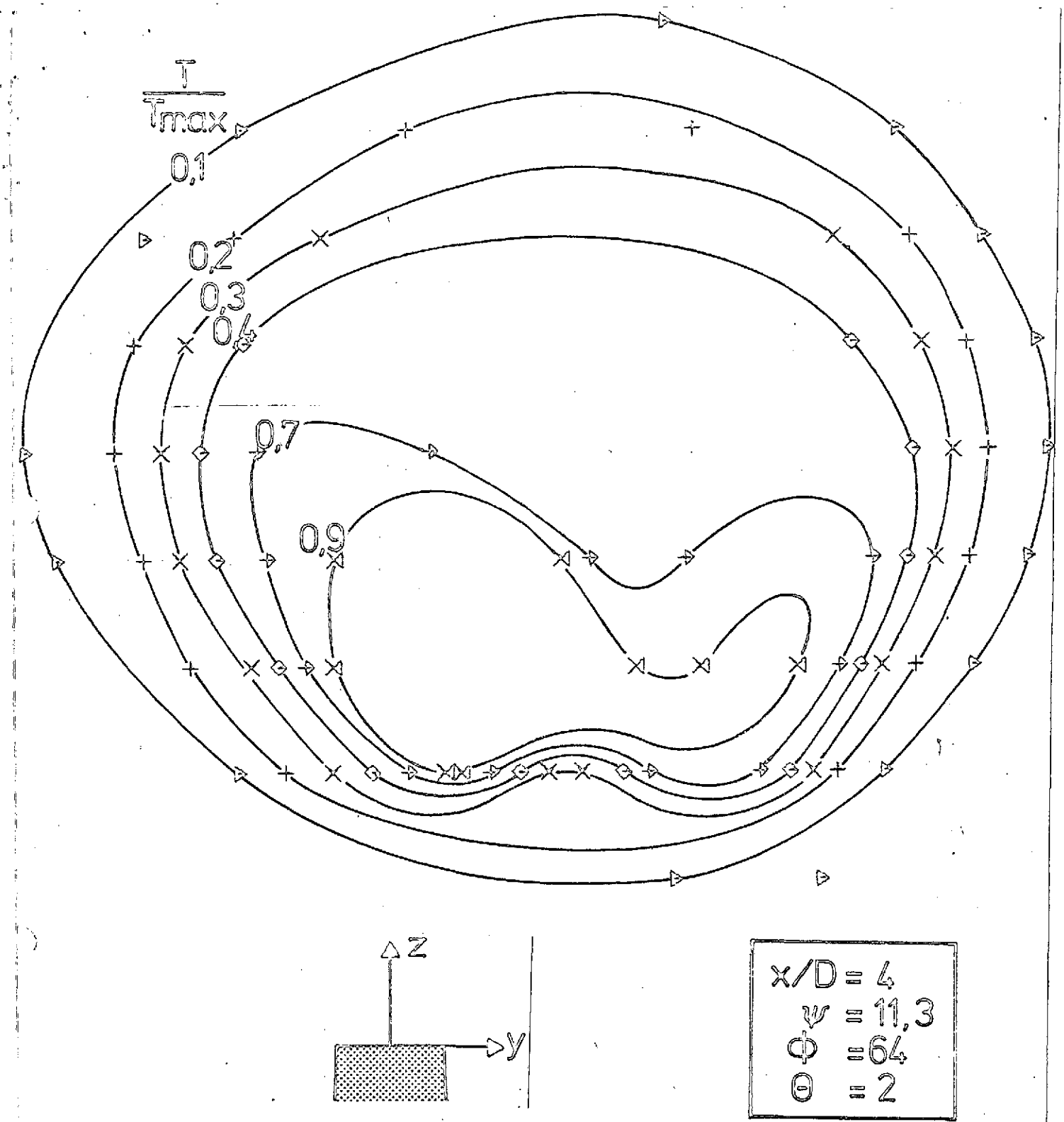

Figure 13. Temperature distribution (isotherms) in the transverse plane (y-z plane) $x/D = 4$, $\psi = 11,3$; $\Phi = 64$, $\Theta = 2$

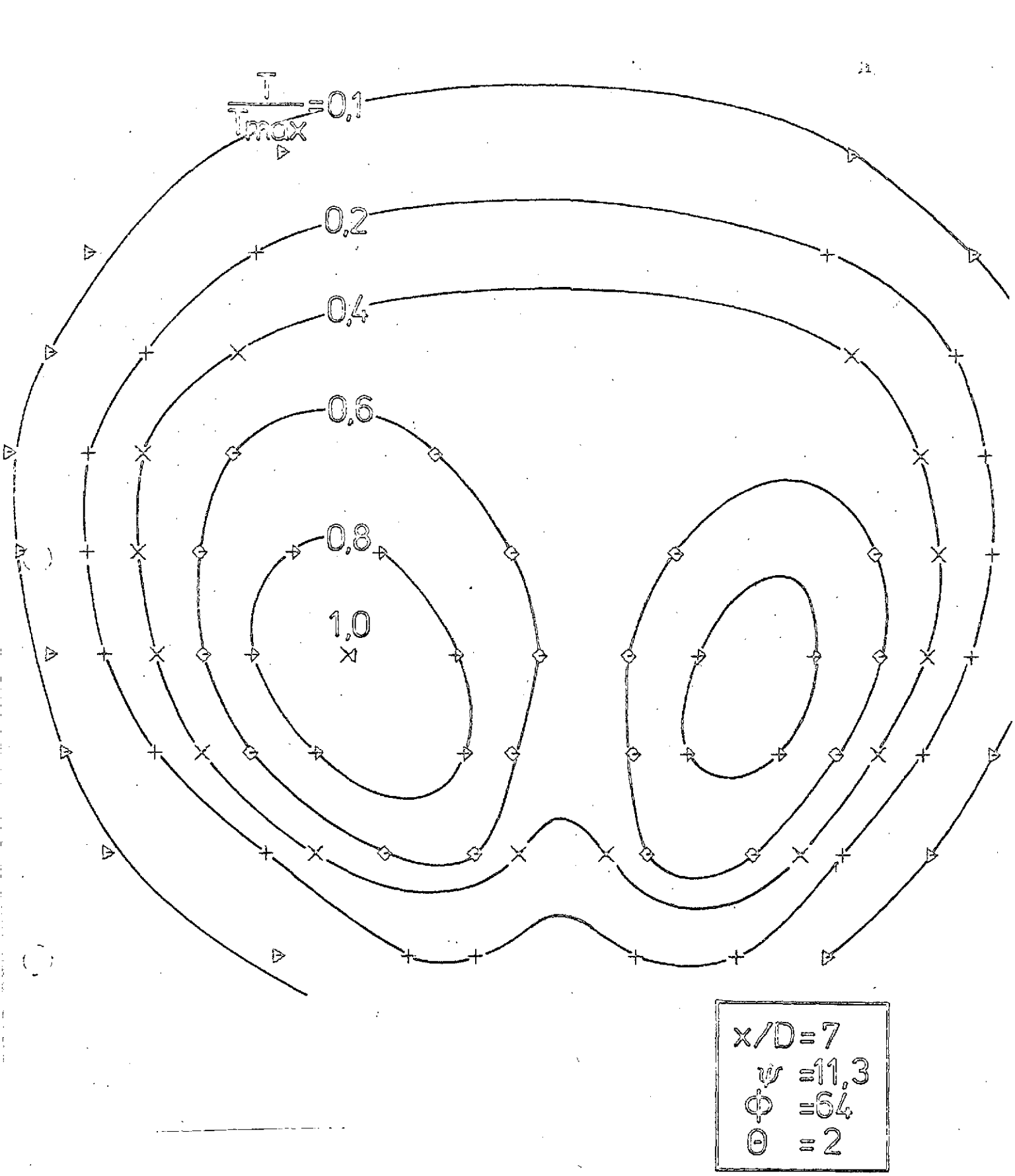

Figure 14. Temperature distribution (isotherm) in the transverse plane (y-z plane) x/D = 7, ψ = 11,3; Φ = 64, Θ = 2

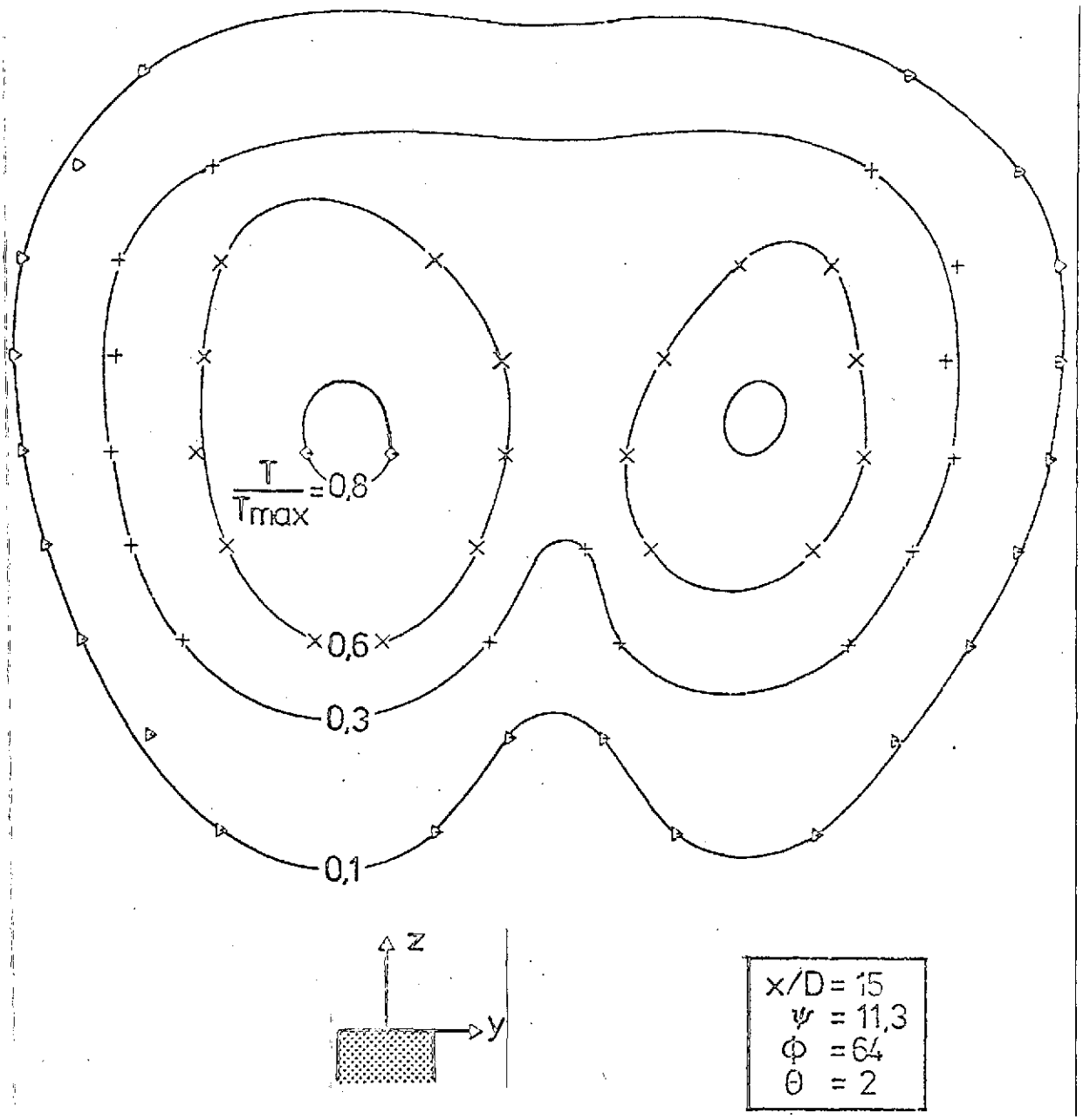

Figure 15. Temperature distribution (isotherm) in the transverse plane (y-z plane) x/D = 15, ψ = 11,3; Φ = 64, Θ = 2

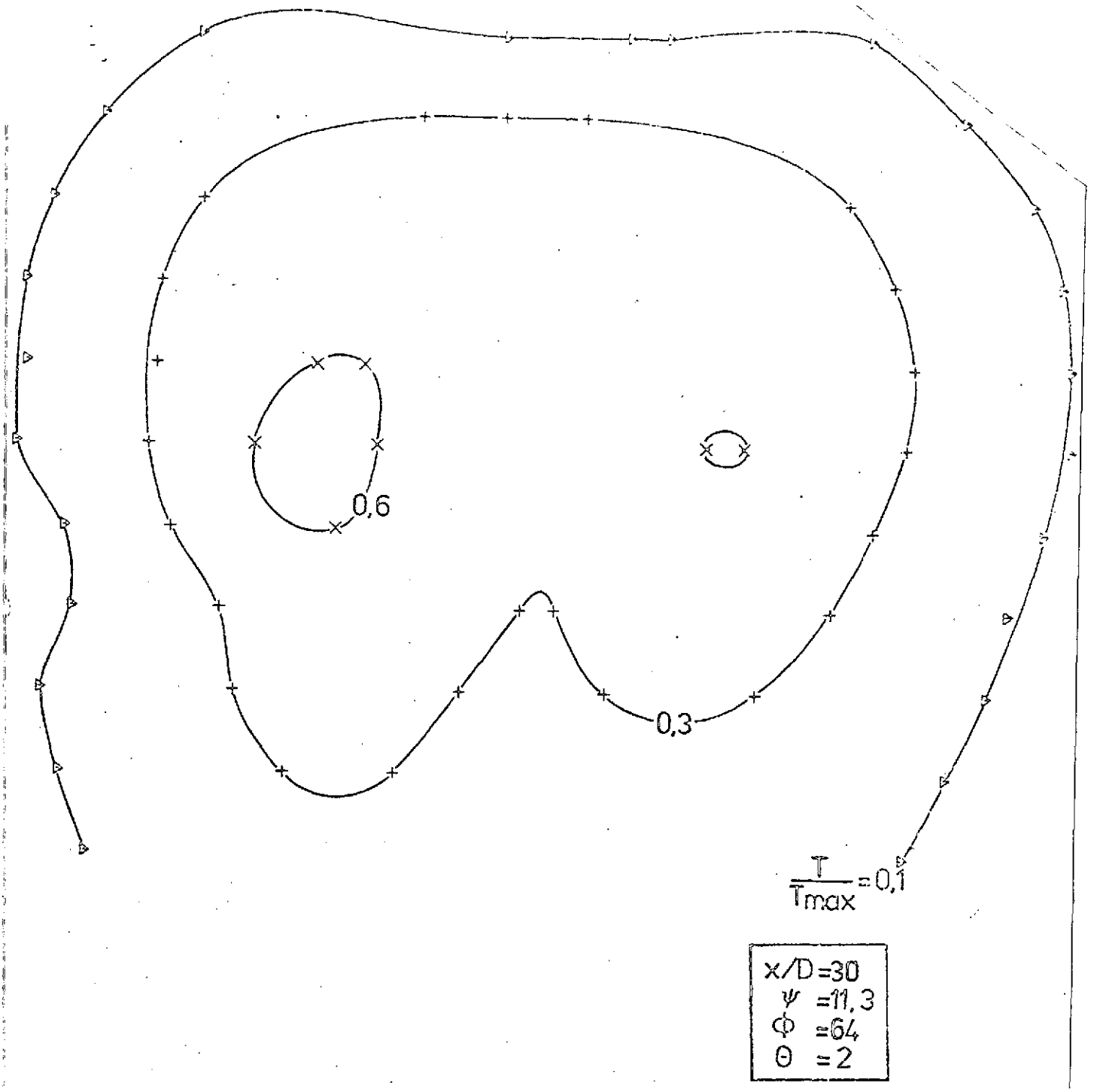

Figure 16. Temperature distribution (isotherm) in the transverse plane (y-z plane) x/D = 30, ψ = 11,3; Φ = 64, Θ = 2

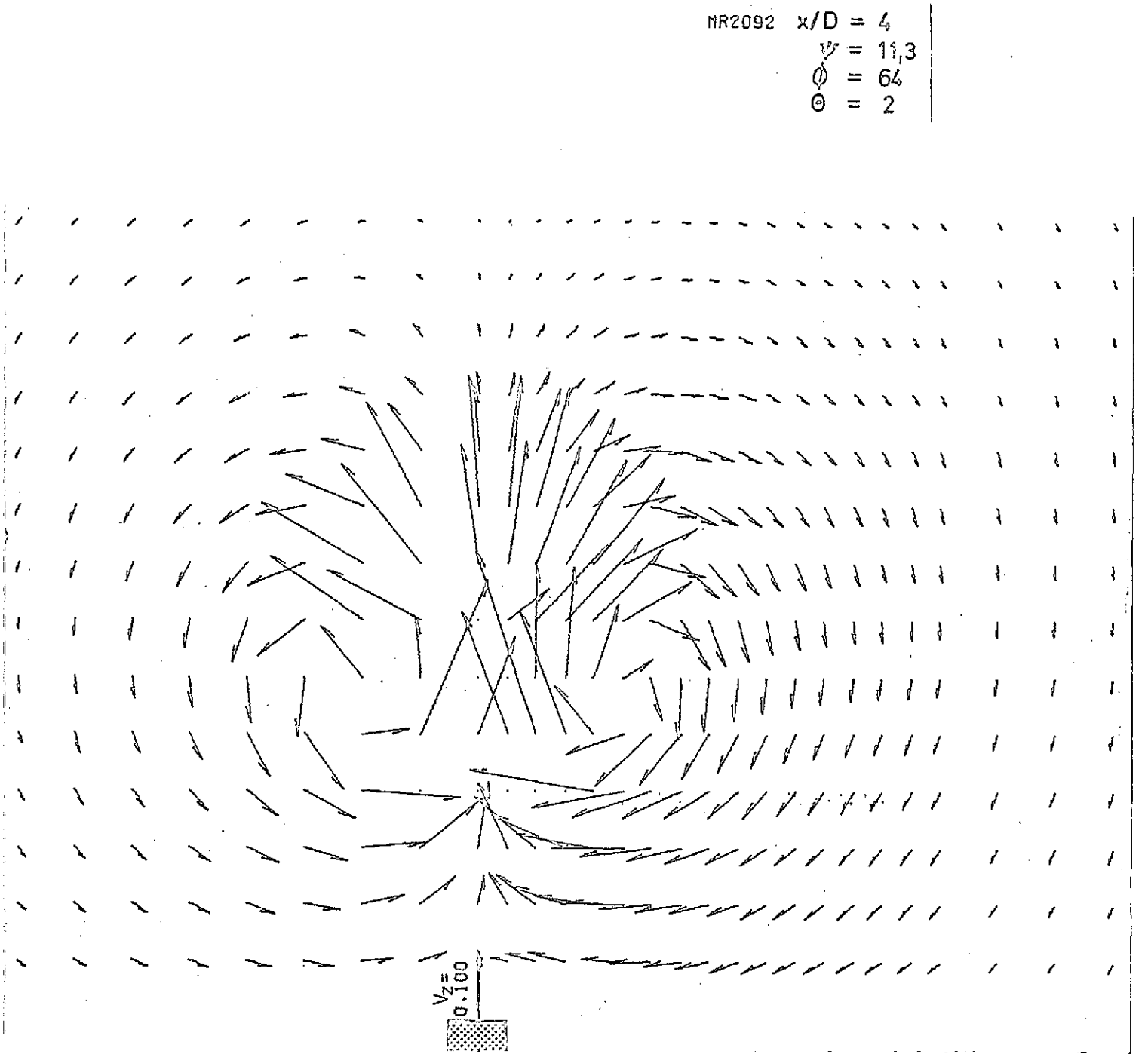

Figure 17. Components of velocity vectors in the transverse plane (y-z plane) for a hot jet $x/D = 4$, $\psi = 11,3$; $\phi = 64$, $\Theta = 2$

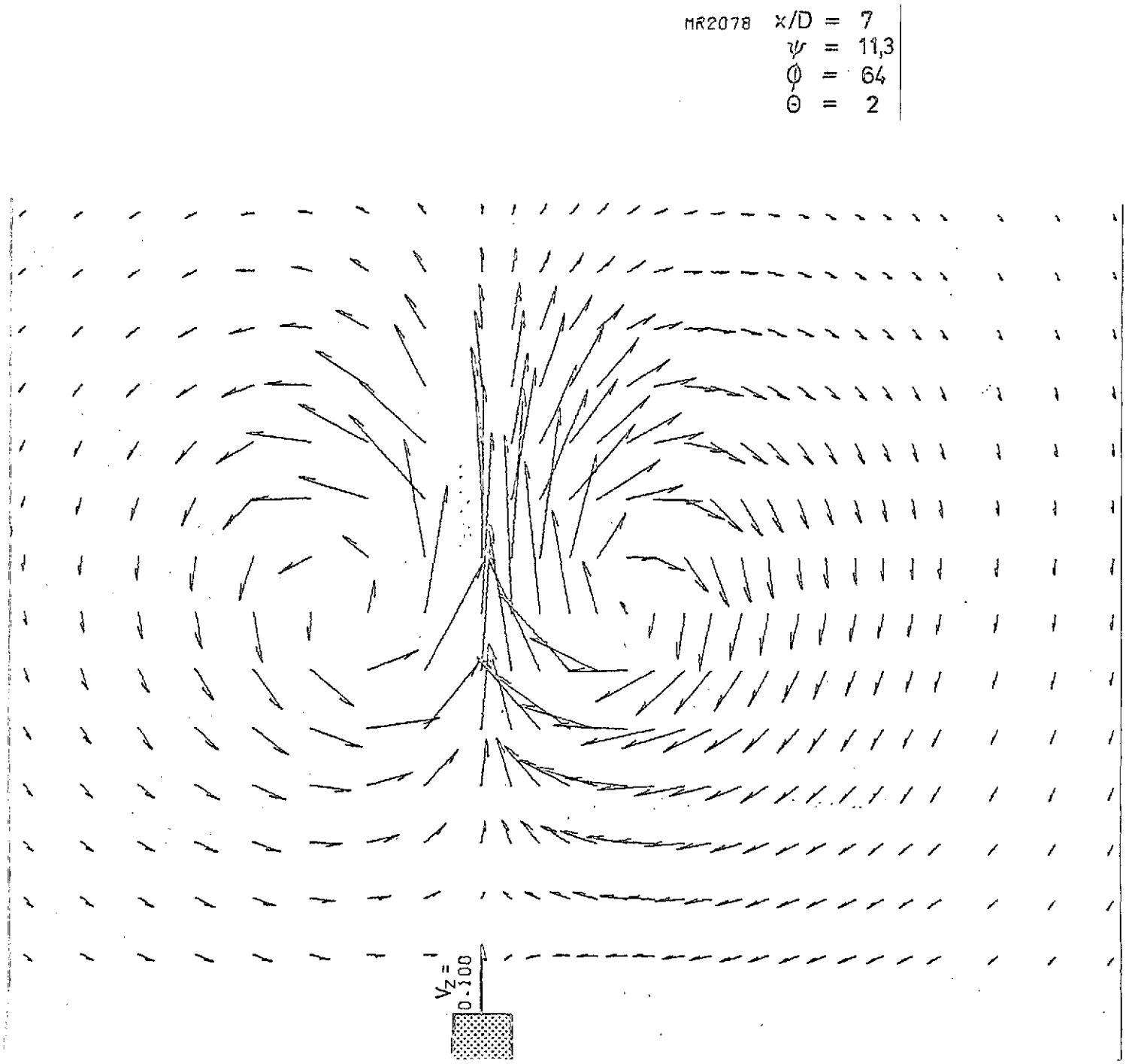

Figure 18a. Components of velocity vectors in the transverse plane (y-z plane) for a hot jet $x/D = 7$, $\psi = 11,3$, $\phi = 64$, $\Theta = 2$

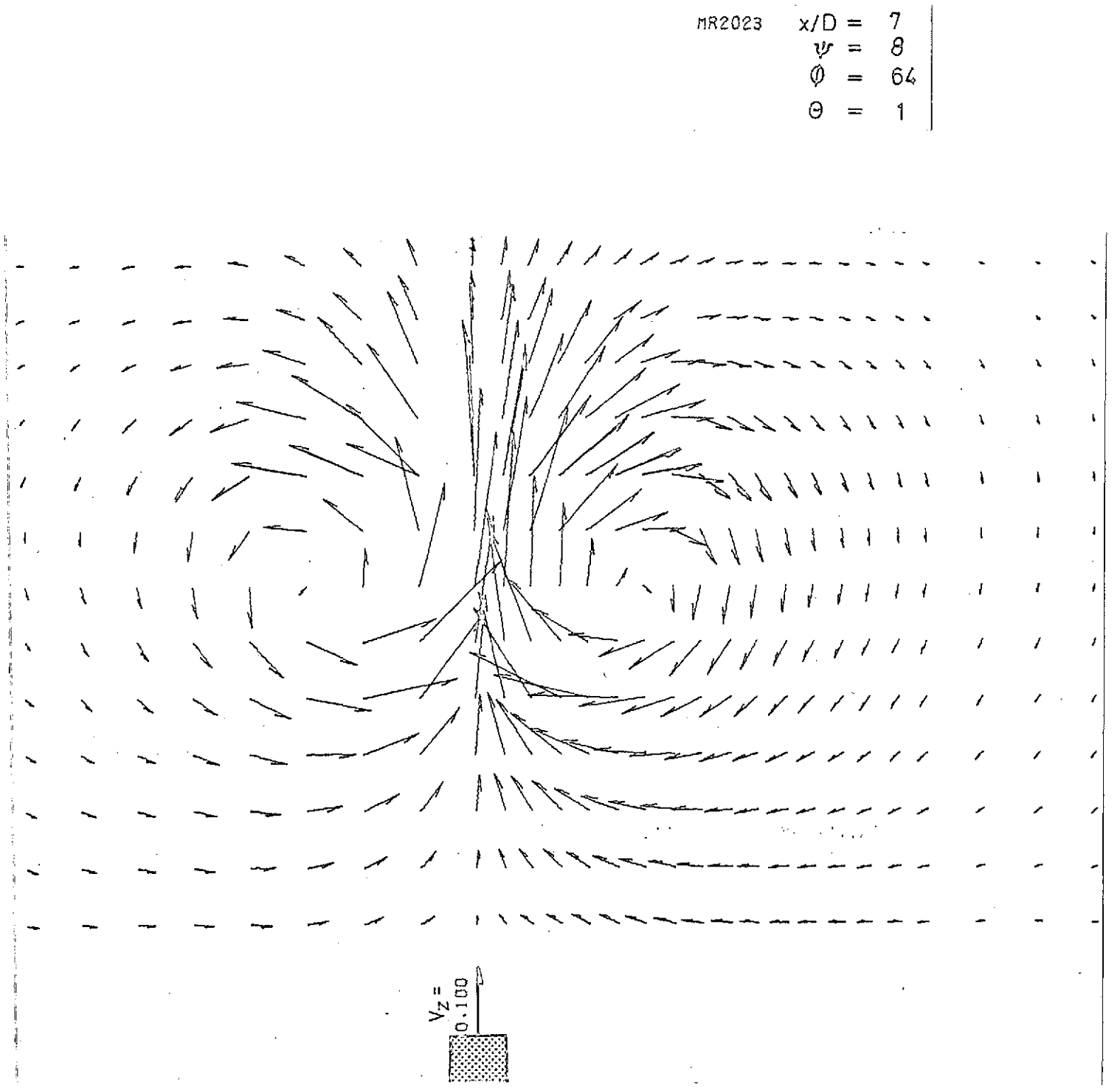

Figure 18b. Components of velocity vectors in the transverse plane (y-z plane) for a hot jet x/D =-7, ψ = 8, φ = 64, Θ = 1

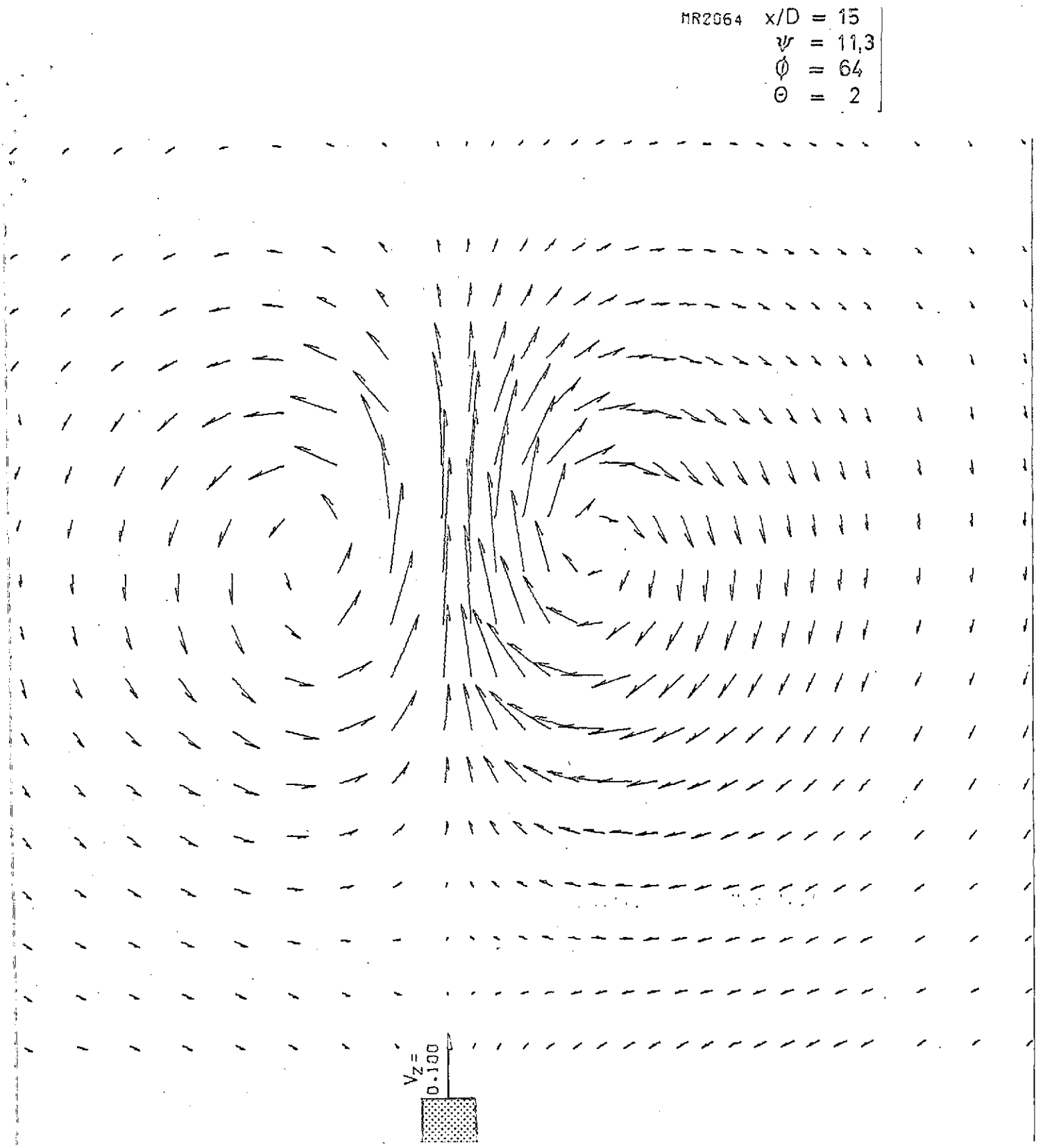

Figure 19a. Components of velocity vectors in the transverse plane (y-z plane) for a hot jet $x/D = 15$, $\psi = 11,3$; $\phi = 64$, $\Theta = 2$

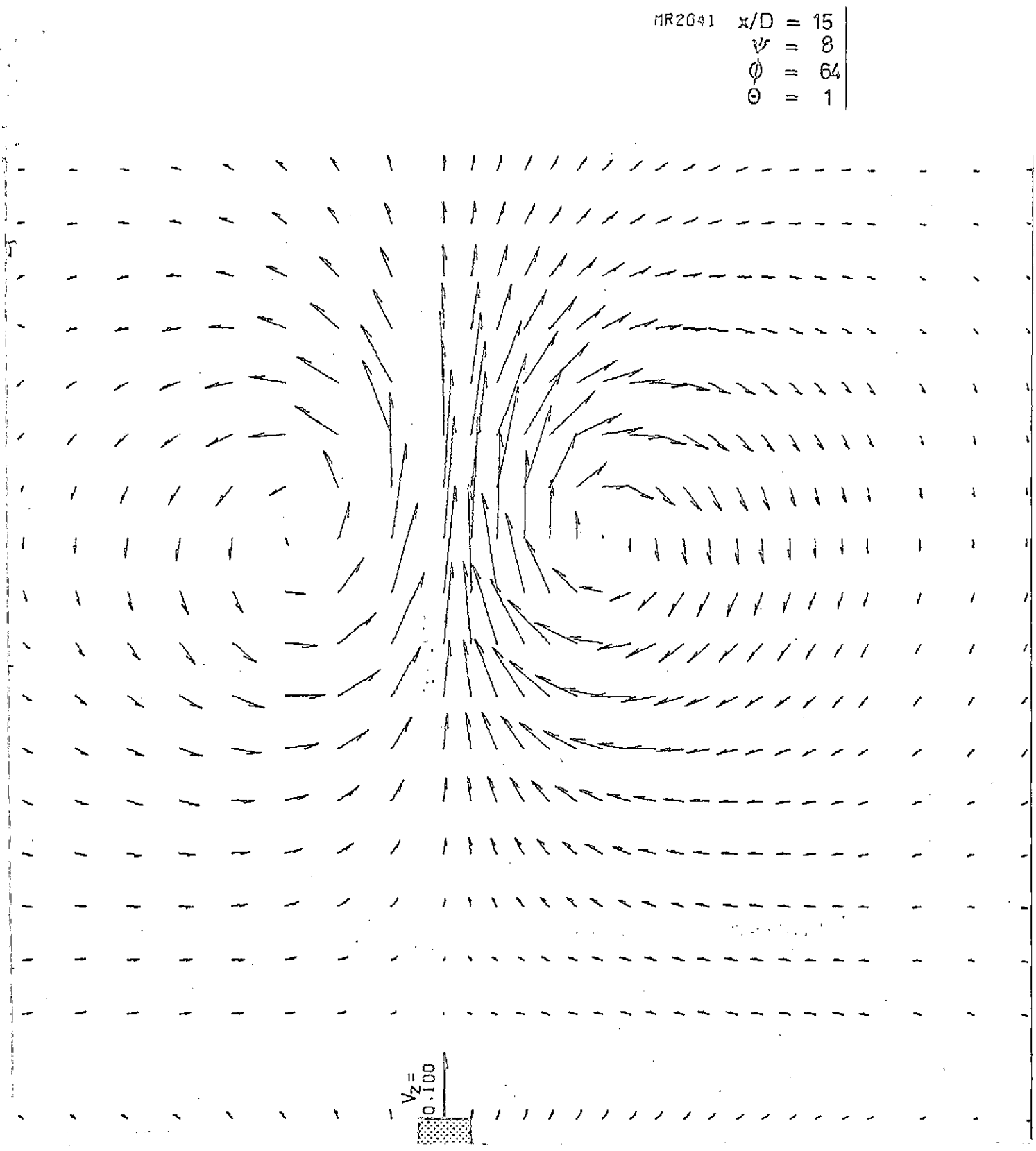

Figure 19b. Components of velocity vectors in the transverse plane (y-z plane) for a hot jet x/D = 15, ψ = 8; ϕ = 64, Θ = 1

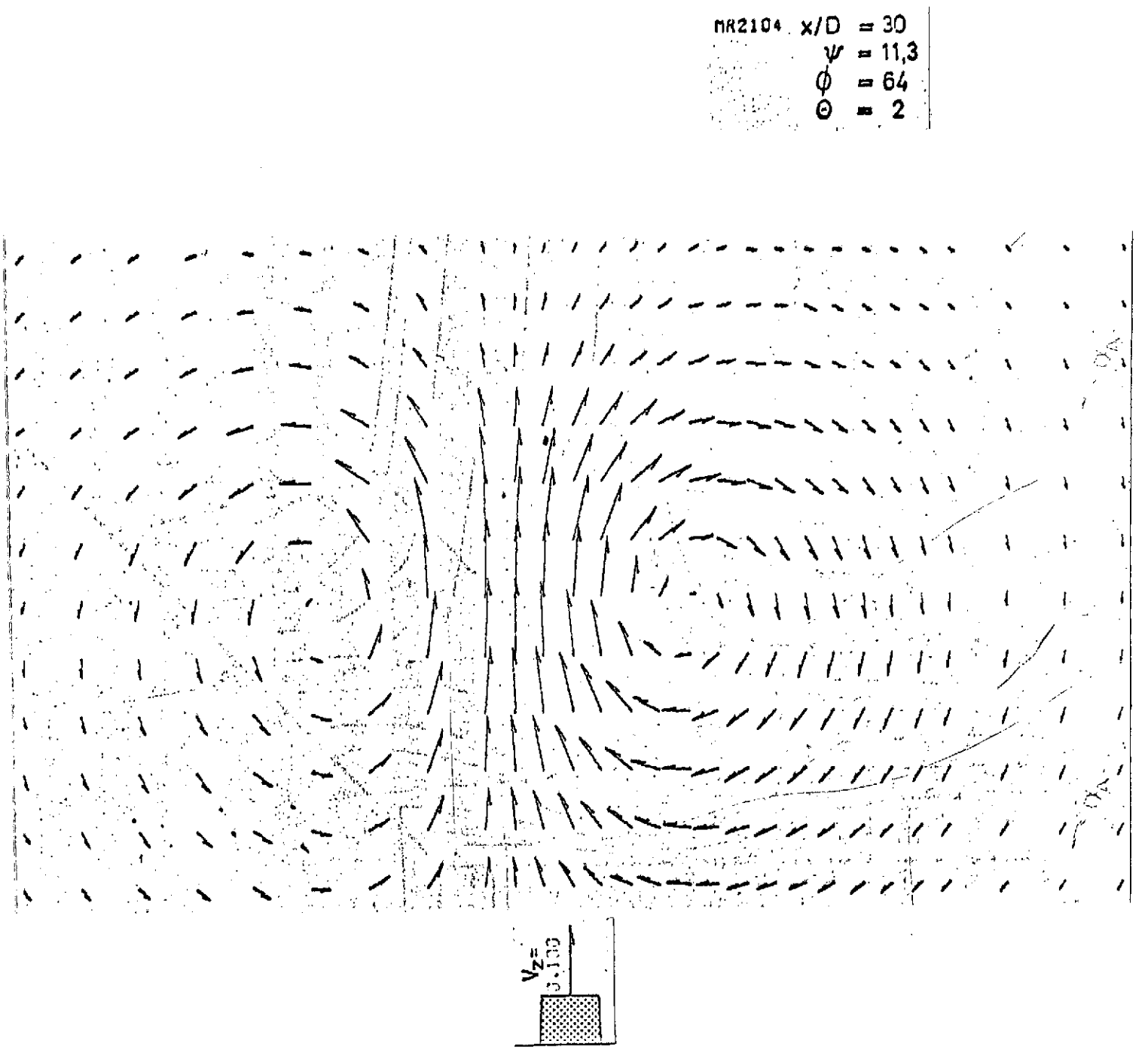

Figure 20. Components of velocity vectors in the transverse plane (y-z plane) for a hot jet x/D = 30, ψ = 11,3; ϕ = 64, Θ = 2

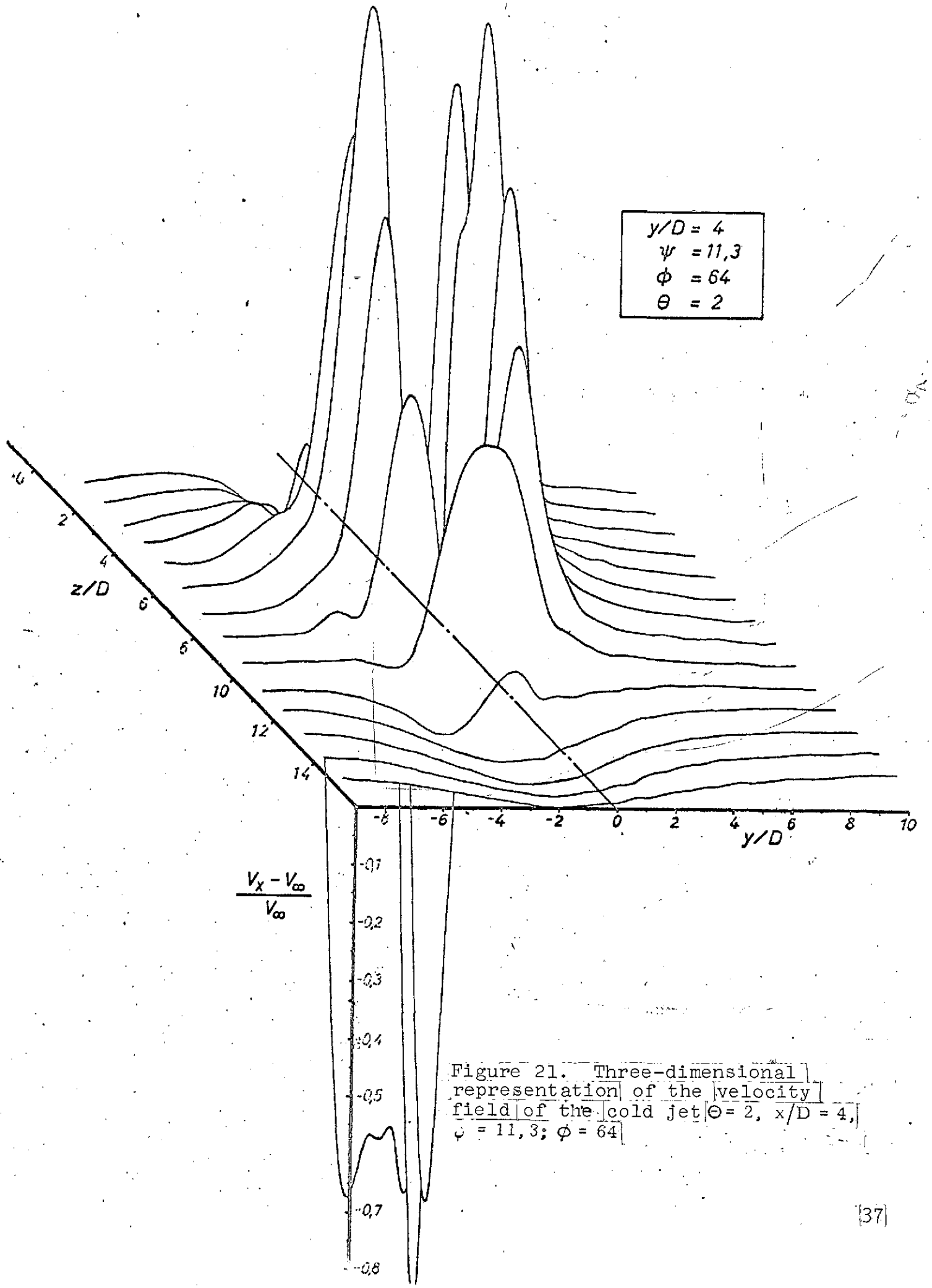

Figure 21. Three-dimensional representation of the velocity field of the cold jet $\Theta = 2$, $x/D = 4$, $\varphi = 11,3$; $\phi = 64$

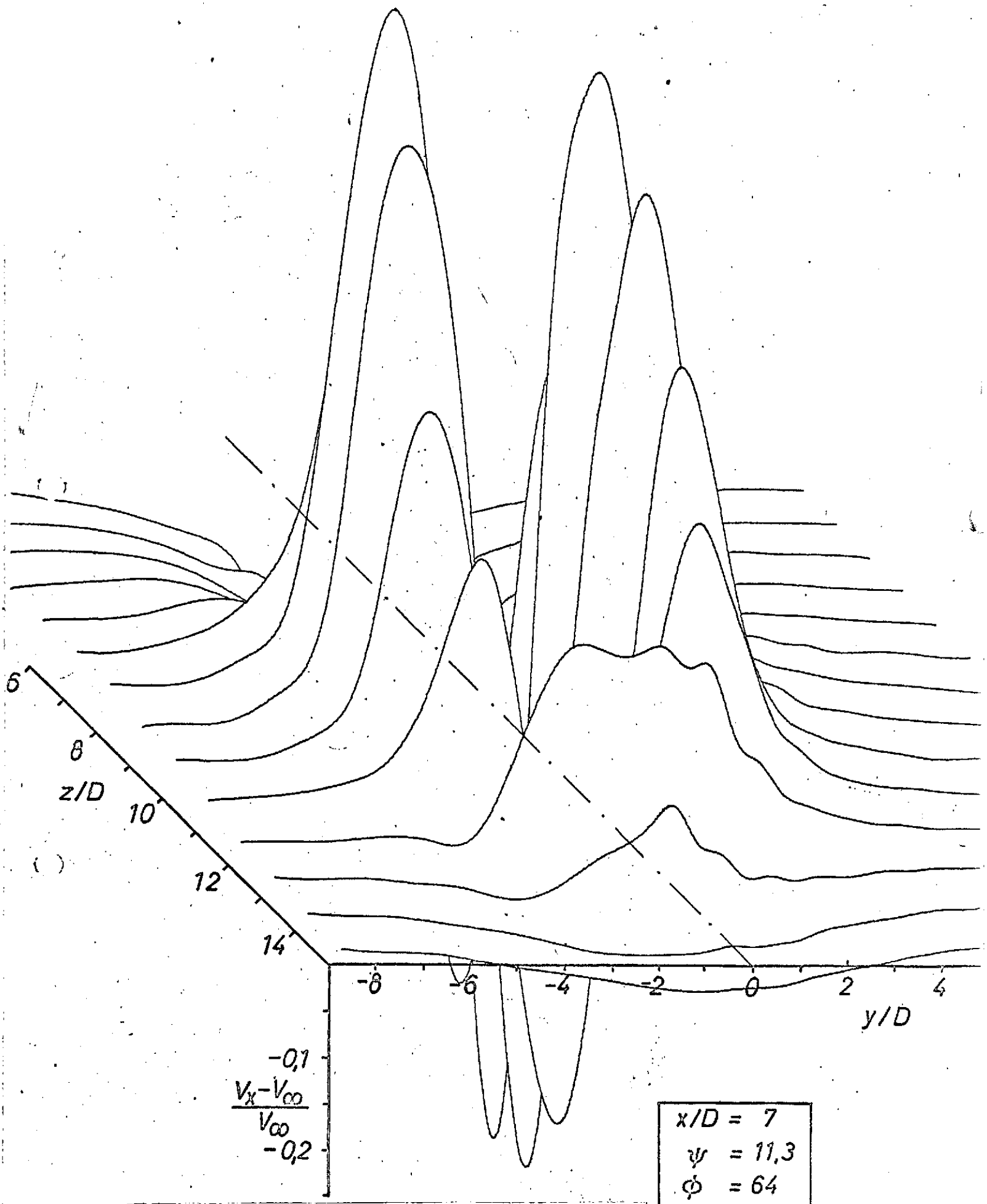

Figure 22a. Three-dimensional representation of the velocity field of the cold jet $\Theta = 2$, $x/D = 7$, $\psi = 11,3$; $\phi = 64$

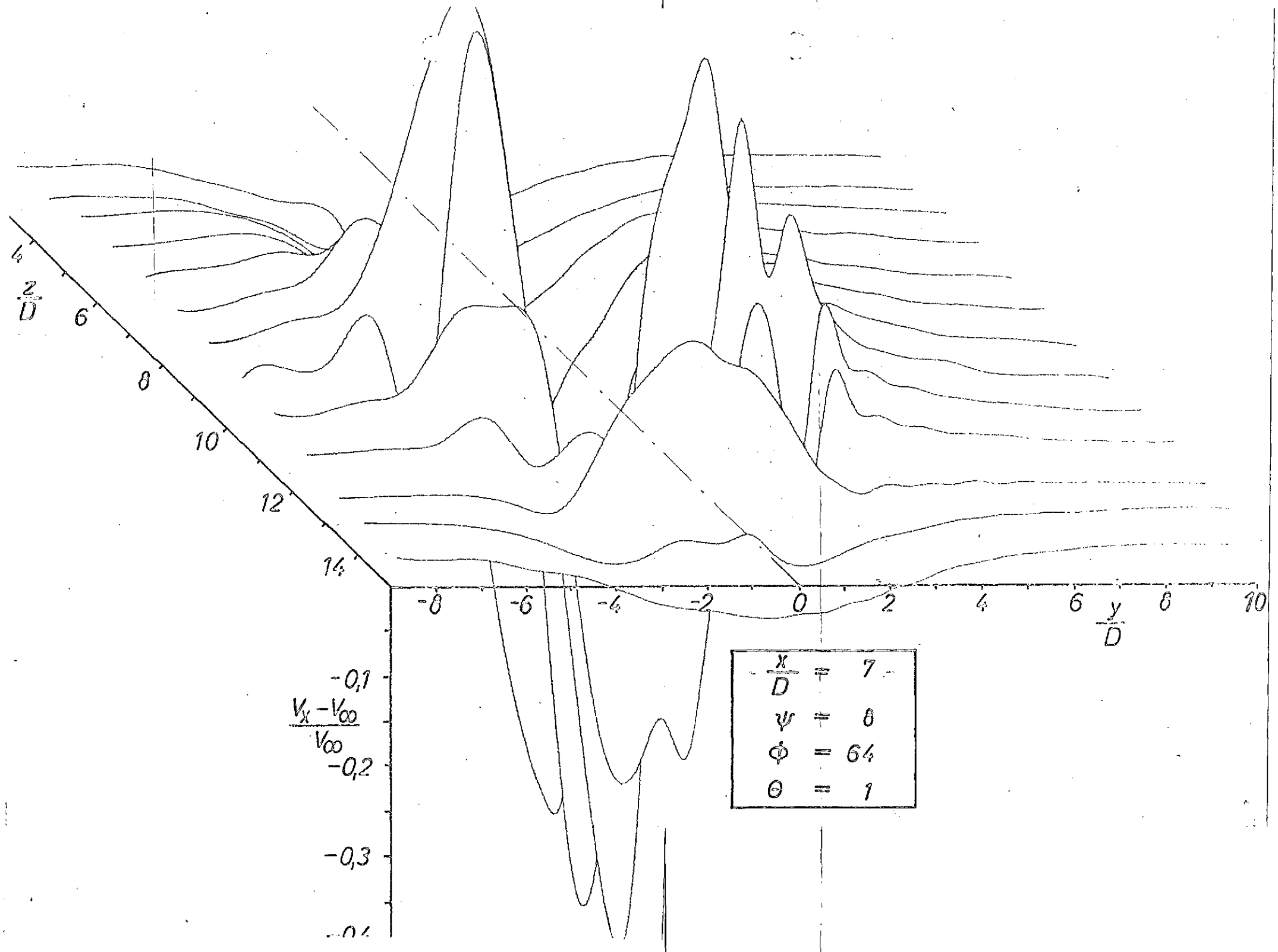

Figure 22b. Three-dimensional representation of the velocity field of the cold jet $\Theta = 1$, $x/D = 7$, $\psi = 8$, $\Phi = 64$

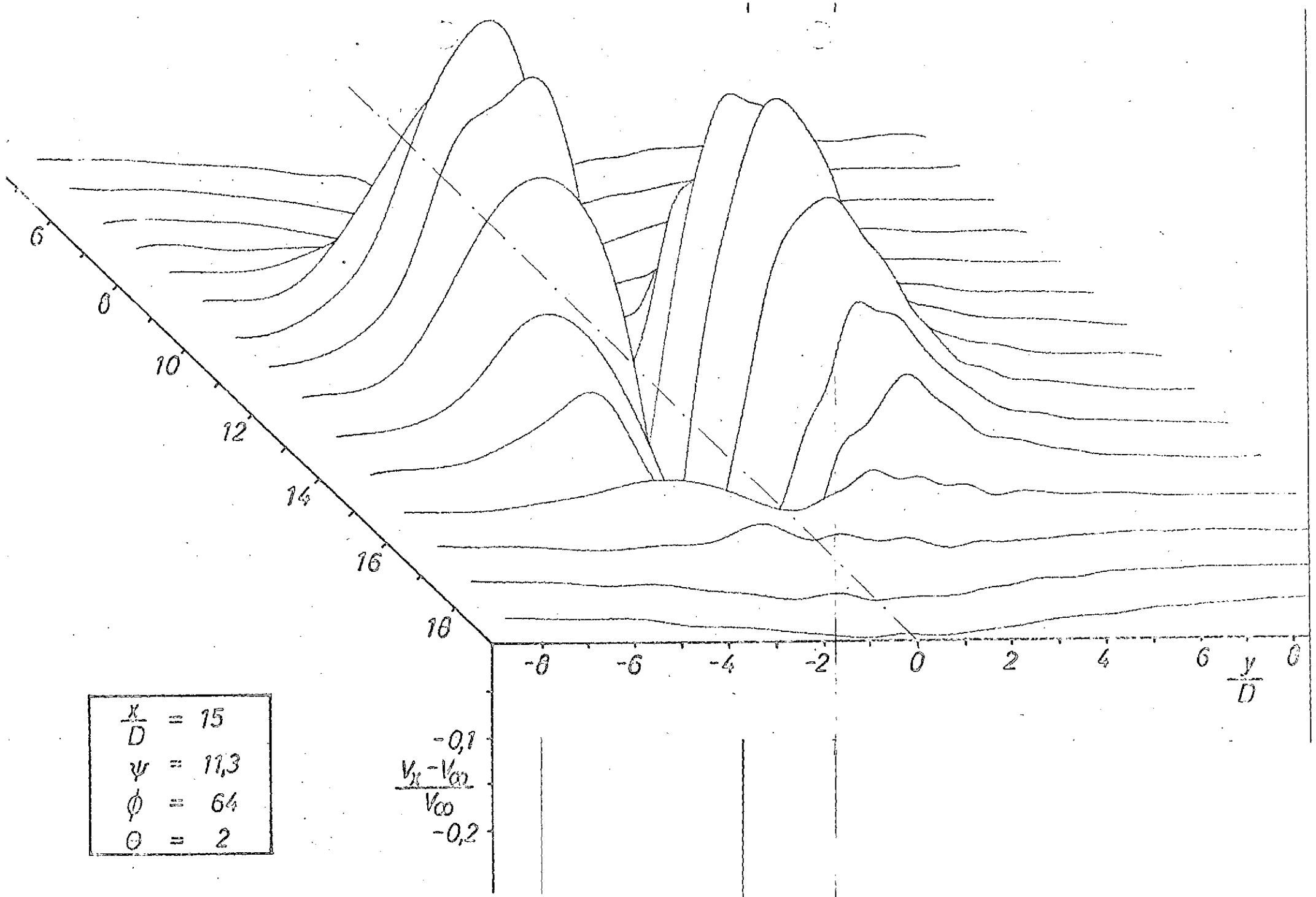

Figure 23a. Three-dimensional representation of the velocity field of the cold jet $\Theta = 2$, $x/D = 15$, $\psi = 11,3$; $\phi = 64$

FOLDOUT FRAME 1

FOLDOUT FRAME 2

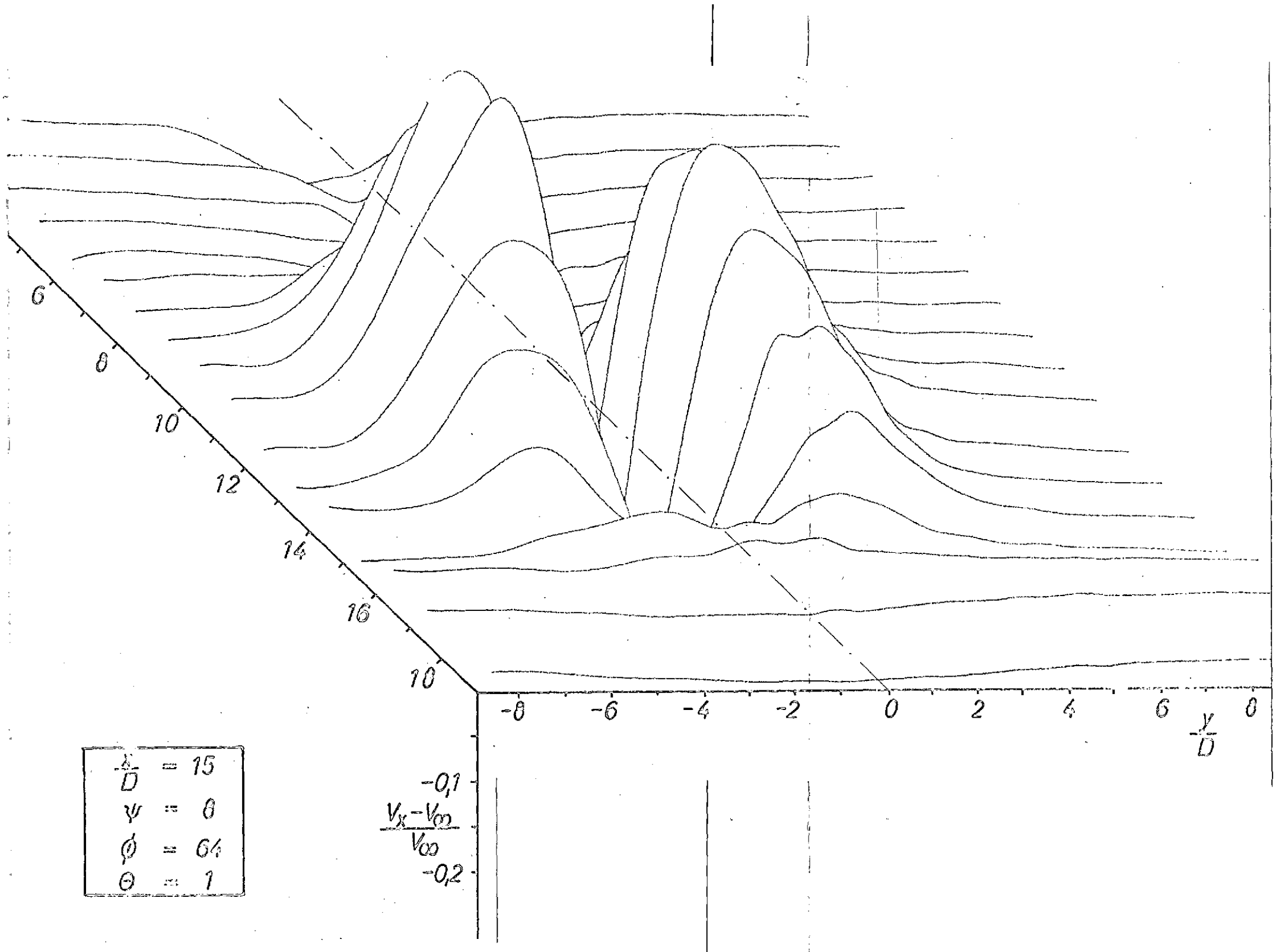

Figure 23b. Three-dimensional representation of the velocity field of the cold jet| $\Theta = 1$, $x/D = 15$, $\psi = 8$, $\phi = 64$|

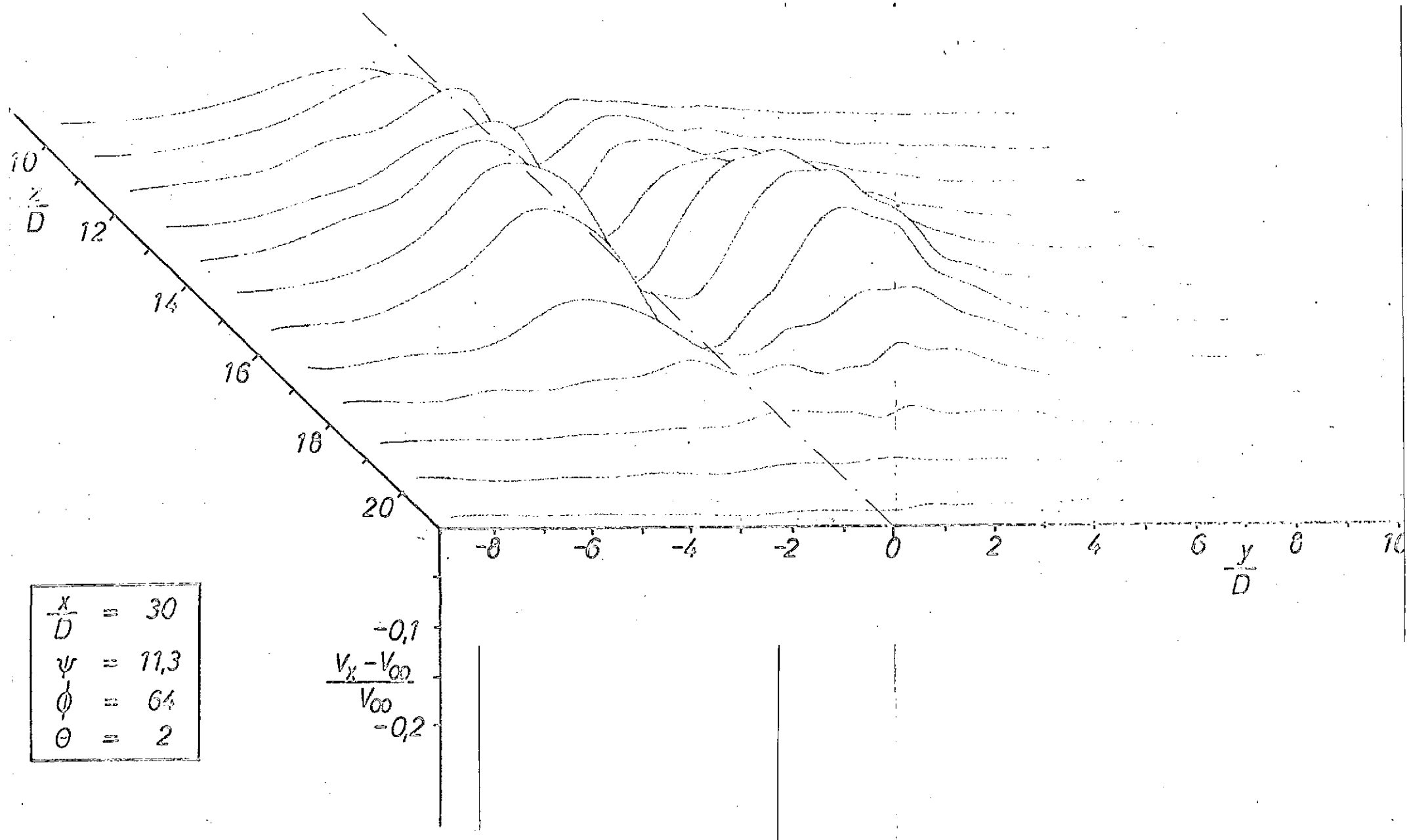

Figure 24. Three-dimensional representation of the velocity field of the cold jet $\Theta = 1$, $x/D = 15$, $\psi = 11,3$; $\varphi = 64$

FOLDOUT FRAME

1

FOLDOUT FRAME

2

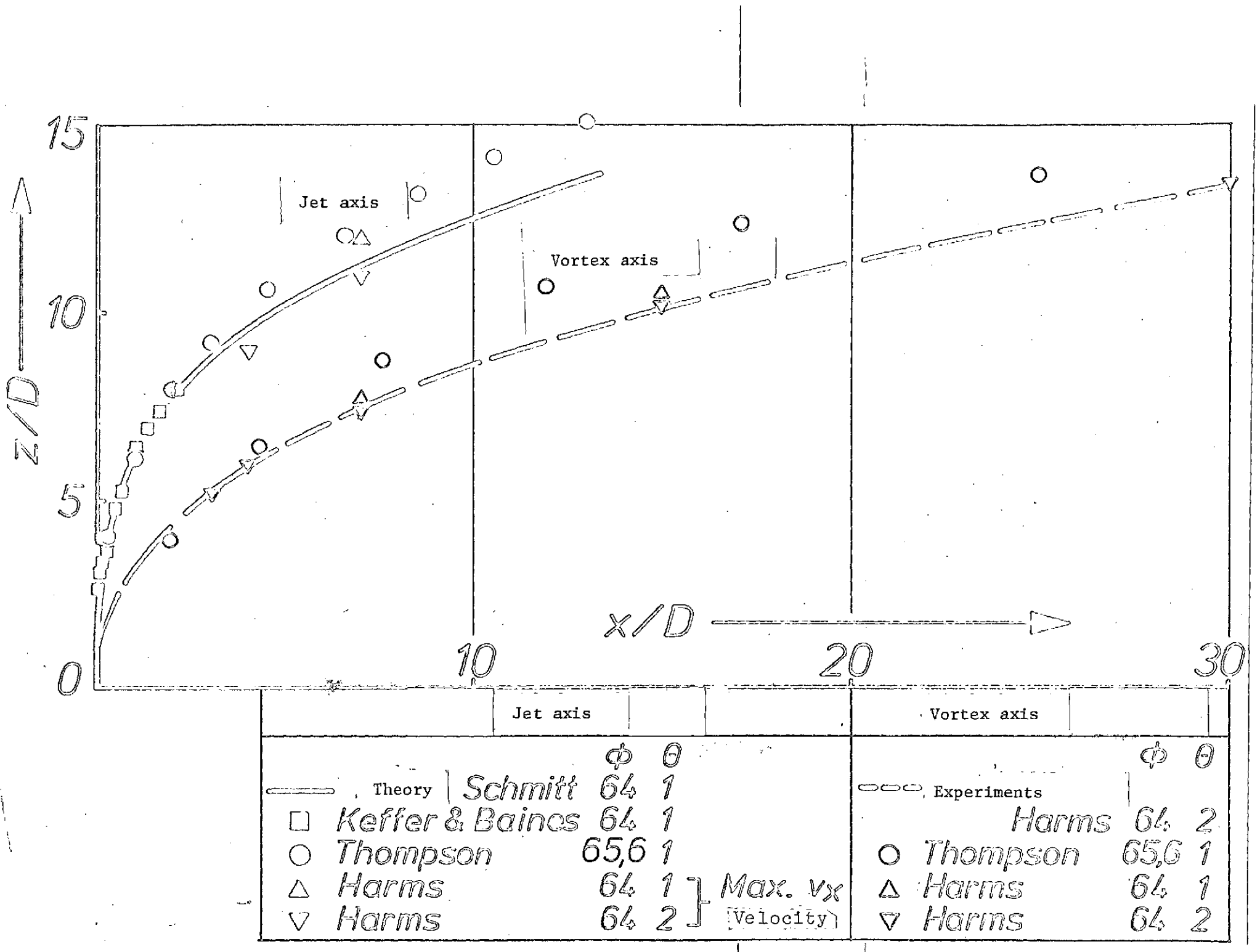

Figure 25. Jet axis and vortex axis

FOLDOUT FRAME

FOLDOUT FRAME